AD-A045 379 AIR FORCE INST OF TECH WRIGHT-PATTERSON AFB OHIO F/G 20/4
LASER STREAK VELOCIMETER FOR TWO-DIMENSIONAL FLOWS IN GASES.(U)
SEP 76 G W SPARKS

UNCLASSIFIED AFIT-CI-77-2 NL

1 OF 1
AD
A045 379

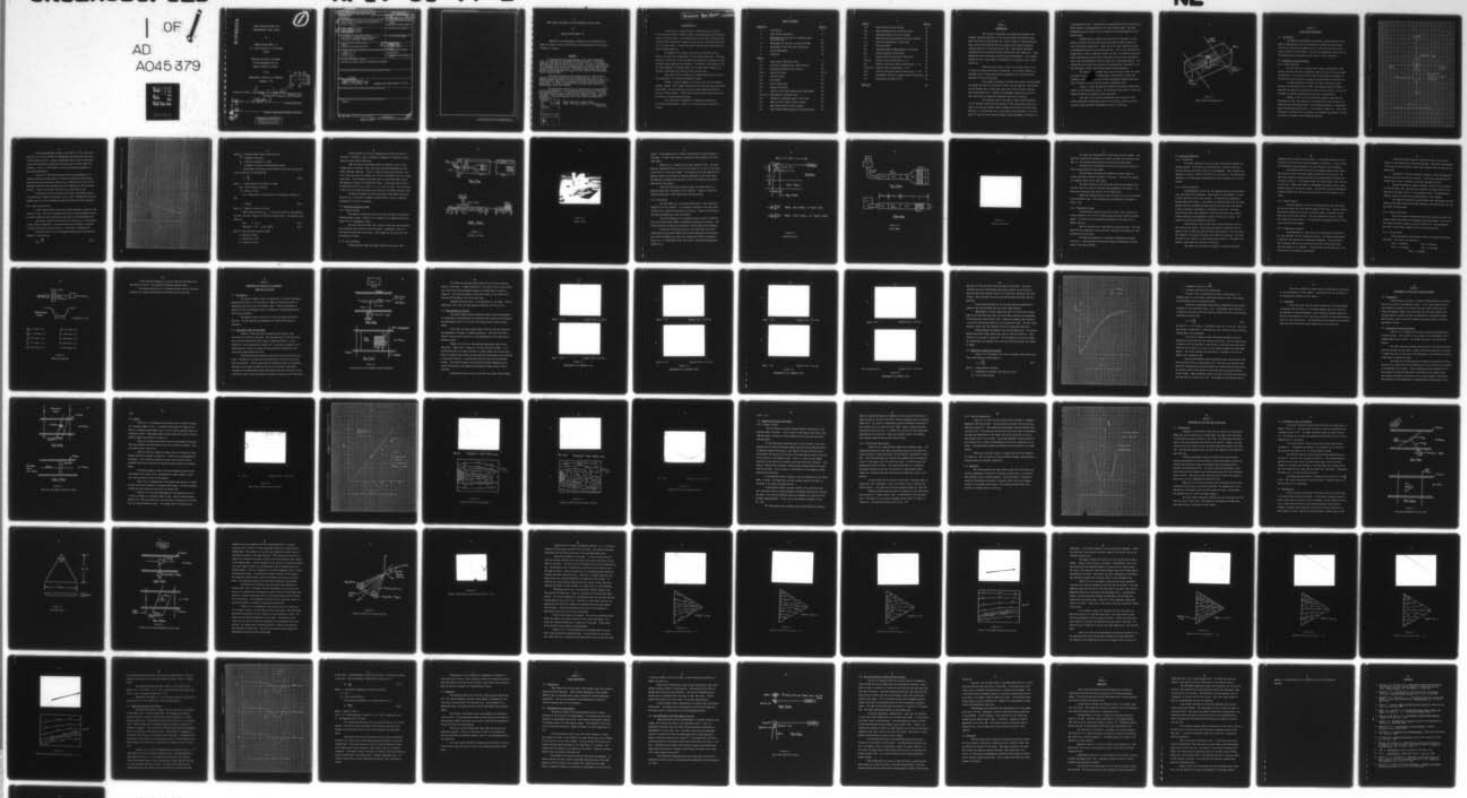

END
DATE FILMED
11-77
DDC

77-2

B.S.

LASER STREAK VELOCIMETER FOR TWO-DIMENSIONAL FLOWS IN GASES

by

GEORGE WILLIAM SPARKS, JR.

B.S., United States Air Force Academy

(1970)

SUBMITTED IN PARTIAL FULFILLMENT

OF THE REQUIREMENTS FOR THE

DEGREE OF MASTER OF SCIENCE

at the

MASSACHUSETTS INSTITUTE OF TECHNOLOGY

September, 1976

Signature of Author George W Sparks Jr

August 16, 1976

Department of Aeronautics and Astronautics

Certified by _____

Thesis Supervisor

Accepted by _____

Chairman, Departmental Graduate Committee

UNCLASSIFIED

SECURITY CLASSIFICATION OF THIS PAGE (When Data Entered)

(14) AFIT REPORT DOCUMENTATION PAGE

READ INSTRUCTIONS BEFORE COMPLETING FORM

1. REPORT NUMBER	2. GOVT ACCESSION NO.	3. RECIPIENT'S CATALOG NUMBER
CI-77-2		(9) Master's Thesis

(6) 4. TITLE (and Subtitle)
Laser Streak Velocimeter for Two-Dimensional Flows in Gases.

5. TYPE OF REPORT & PERIOD COVERED
Thesis

6. PERFORMING ORG. REPORT NUMBER

(10) 7. AUTHOR(s)
GEORGE W. SPARKS, JR
CAPTAIN, USAF

8. CONTRACT OR GRANT NUMBER(s)

9. PERFORMING ORGANIZATION NAME AND ADDRESS
AFIT Student at Massachusetts Institute of Technology, Cambridge, Massachusetts

10. PROGRAM ELEMENT, PROJECT, TASK AREA & WORK UNIT NUMBERS

11. CONTROLLING OFFICE NAME AND ADDRESS
AFIT/CI
Wright-Patterson AFB OH 45433

(11) 12. REPORT DATE
September 1976

13. NUMBER OF PAGES
81 pages

14. MONITORING AGENCY NAME & ADDRESS (if different from Controlling Office)
(12) 82 p.

15. SECURITY CLASS. (of this report)
Unclassified

15a. DECLASSIFICATION/DOWNGRADING SCHEDULE

16. DISTRIBUTION STATEMENT (of this Report)
Approved for Public Release; Distribution Unlimited

17. DISTRIBUTION STATEMENT (of the abstract entered in Block 20, if different from Report)

18. SUPPLEMENTARY NOTES
JERRAL F. GUESS, Captain, USAF
Director of Information, AFIT
APPROVED FOR PUBLIC RELEASE AFR 190-17.

19. KEY WORDS (Continue on reverse side if necessary and identify by block number)

20. ABSTRACT (Continue on reverse side if necessary and identify by block number)
Attached

DD FORM 1 JAN 73 1473 EDITION OF 1 NOV 65 IS OBSOLETE

UNCLASSIFIED

SECURITY CLASSIFICATION OF THIS PAGE (When Data Entered)

012200

LASER STREAK VELOCIMETER FOR TWO-DIMENSIONAL FLOWS IN GASES

by

GEORGE WILLIAM SPARKS, JR.

Submitted to the Department of Aeronautics and Astronautics on August 16, 1976, in partial fulfillment of the requirements for the degree of Master of Science.

ABSTRACT

A new velocity measuring technique, laser streak velocimetry (LSV), was developed for two-dimensional flows in gases. A high power argon ion laser beam was formed into a thin sheet of light to illuminate a two-dimensional plane in the flow around a body. Ten micron sized particles were introduced into the flow, and photographs were taken of the particles as they traversed the light sheet. The length of the streak made by each particle on the photograph was a measure of its velocity since the camera shutter speed was known.

The velocity profile in the boundary layer of a flat plate was measured and found to agree within 4% of the theoretical value. Low Reynolds number flow around a circular cylinder was measured, and velocities in the wake were found in close agreement with theory and with previous measurements. A velocity mapping of the non-steady vortex shedding of a Karman vortex street was also made.

The flow around a delta wing was analyzed due to current interest in low speed separation. The velocities above the surface of a 60° delta wing were measured by LSV, and results were compared to theory. The flow was found to be non-conical, contrary to the assumption of most analytical treatments. Future developments of the laser streak velocimeter were discussed.

Thesis Supervisor: Shaoul Ezekiel
Title: Associate Professor of Aeronautics and Astronautics

ACKNOWLEDGEMENTS

I would like to extend my deepest appreciation to my advisor, Professor Shaoul Ezekiel, without a doubt, the most brilliant and dedicated person I have ever known. His innate ability to see right to the heart of a problem and to immediately suggest a solution, was a continual motivation for me to work harder. I hopefully depart a better person and engineer for having studied under him.

The people of the Research Laboratory of Electronics were a pleasure to work with, professionals in every sense of the word. This goes especially for the men in the lab, whose good humor and willingness to help, provided a great atmosphere for research. Dick Hackel, Sully Balsamo, Fred Wu, Steve Goldstein, and Kambiz Alavi will be famous names someday, so I document it here that they were my friends way back then.

Anne Clee has done a superb job of converting my draft into this fine manuscript. She receives my heartfelt thanks.

Finally, a special thought for my wife, Karyn, and our newborn daughter, Rachel. Their support and patience over the last year were deeply appreciated. The long evenings of work and study seemed more pleasant because of their presence. Rachel even did her part by keeping me up late at night so I could get more work done.

This research was conducted in the Research Laboratory of Electronics and sponsored, in part, by the Joint Services Electronics Program.

TABLE OF CONTENTS

Chapter 1

INTRODUCTION

The science of aeronautics has always been plagued by the somewhat intangible qualities of air and the problems of measuring these qualities without disturbing the flow. Early systems for velocity measurement, such as pitot tube and hot wire systems, were accurate enough but required probes to be inserted into the flow. These probes invariably disturbed the flow, particularly when inserted near other bodies [1]. These methods were also restricted to point-by-point measurements. This required steady flow and a large number of measurements to accurately cover a large flow field.

While smoke was used as a tracer to visualize flows in air, it could not provide any velocity information. It was always treated as a continuum since it could not be easily broken down into individual smoke particles to trace the flow [8].

Laser doppler velocimetry increased the accuracy of measurements and negated the need for insertion of probes into the flow [2]. While there are LDV systems with a limited scan rate, most are restricted to point-by-point measurements [16]. A method of simultaneously measuring velocities over large areas was needed for nonsteady flows such as vortices.

The technique used in this thesis, laser streak velocimetry or LSV, although lacking the high accuracy of LDV, solved most of the problems of the previous methods without introducing any major new difficulties. Basically, it involved the use of a high power laser to produce a very thin sheet of light that was used to construct streak photographs of particles in

a two-dimensional plane. The velocity was determined by dividing the particle streak length on the photographs by the camera shutter speed. Direction information was also clearly visible, making it an alternate method of flow visualization.

Although particle tracers have been used for many years in aeronautical research, they have been mostly restricted to water tunnels and flow visualization schemes [8]. Tracer use in air flows required particles of approximately micron size to follow the flow. This in turn required high energy density light to record the streaks on film. The advent of high power lasers provided an excellent light source that could be easily transformed into a thin, two-dimensional sheet of light with a high energy density. This allowed the use of very small particles at concentrations low enough to prevent individual streaks from running together on the photograph.

The laser beam was formed into a very thin sheet (<1mm) that could be placed in any orientation around a body. While sheets of light from incoherent sources have been used in flow visualization schemes previously, their thickness was limited to the order of centimeters [15].

Figure 1-1 shows the general technique for producing streak photographs of a two-dimensional plane. The velocity of each streak is the streak length divided by the exposure time of the camera.

This thesis will discuss the apparatus and procedure of laser streak velocimetry; measurements made on a flat plate, circular cylinder, and delta wing; and future developments possible in this area.

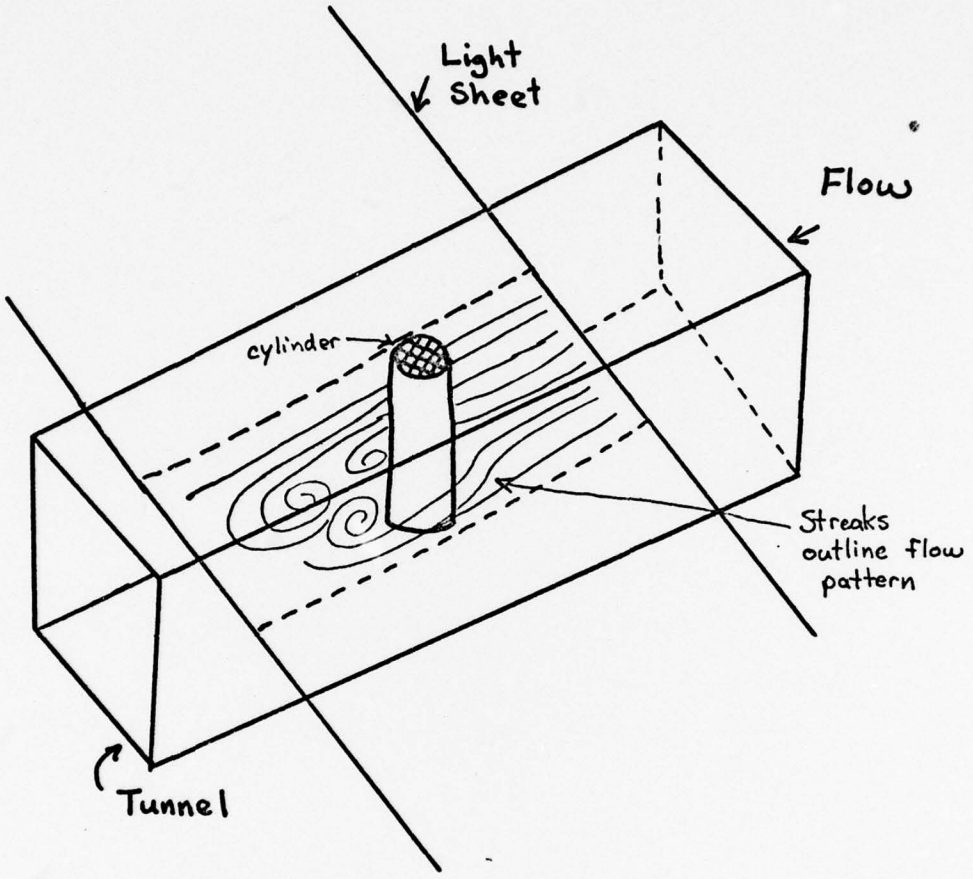

Figure 1-1

LASER STREAK VELOCIMETRY SETUP

Chapter 2

LASER STREAK VELOCIMETRY

2.1 Introduction

An important consideration in devising a streak technique for air flows is what type and size of particles will scatter light efficiently, while still following flow patterns in air. These two areas will be discussed initially in this chapter. This will be followed by a description of the apparatus and the procedures used in laser streak velocimetry.

2.2 Properties of Small Particles

2.2.1 Light Scattering

The fact that this technique uses streaks on photographic film requires that the particles be efficient light scatterers at the wavelength of light used. This can basically be satisfied by having the diameter of the particles more than twice as large as the wavelength of the light [3].

A complete analytical solution for light scattering by small particles was developed by Mie in 1908. His analysis began with Maxwell's equations and applied the appropriate boundary conditions [4]. As such, his treatment is extremely complicated and will not be covered here.

However, as the size of the particles becomes larger than the wavelength of light, the scattering can be broken down into two parts, the diffracted and reflected portions. The diffraction pattern is concentrated about a bright central lobe near $\theta = 0$, as shown in Figure 2-1. The reflected light is scattered in all directions in a definite lobe pattern, no part of which is as bright as the diffracted lobe [4].

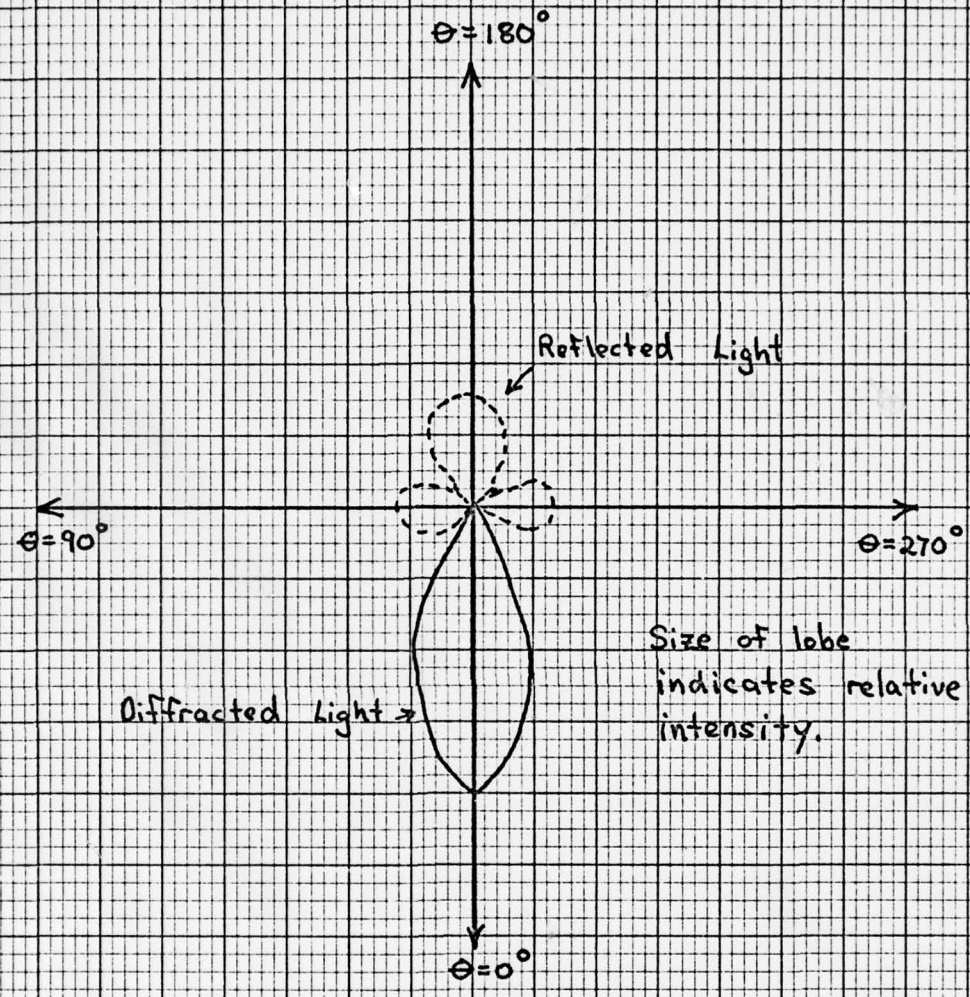

Figure 2-1

DIVISION OF SCATTERING BY A SMALL PARTICLE

Since the photographic data was all taken at $\theta = 90°$, there was a great deal less light available for photographs than there would have been in the diffracted region. However, photographs made at such a large angle to the flow would have introduced major distortions in streak length and direction. At the $\theta = 90°$ position, little distortion was apparent on a test pattern photograph.

Since the $\theta = 90°$ position appears best for photography, it is imperative that the maximum amount of light be reflected by the particles. The normalized scattering cross section, K_s, is defined as the ratio of the apparent scattering cross-sectional area to the geometrical cross-sectional area [5]. Figure 2-2 shows the variation of K_s with particle size.

The particles used in this work had a normal distribution around a 10 micron mean diameter, giving them a K_s of 2 [5]. Although less than the maximum value of 5, this nevertheless makes them efficient light scatterers.

2.2.2 Small Particle Flow

A basic factor governing the use of small particles is how well they follow the flow. The flow of suspended particles has been thoroughly studied by several people and their results have been used in LDV measurements [3].

The classic solution for the motion of a particle in a fluid medium is that given by Stokes [6]. It has been shown that the Stokes' treatment is highly accurate for particle sizes of .1-10 microns in diameter [7].

For particles this size, the Reynolds number based on the particle diameter is less than one.

$$R_{e_p} = \frac{dV_p}{\nu} \tag{2.1}$$

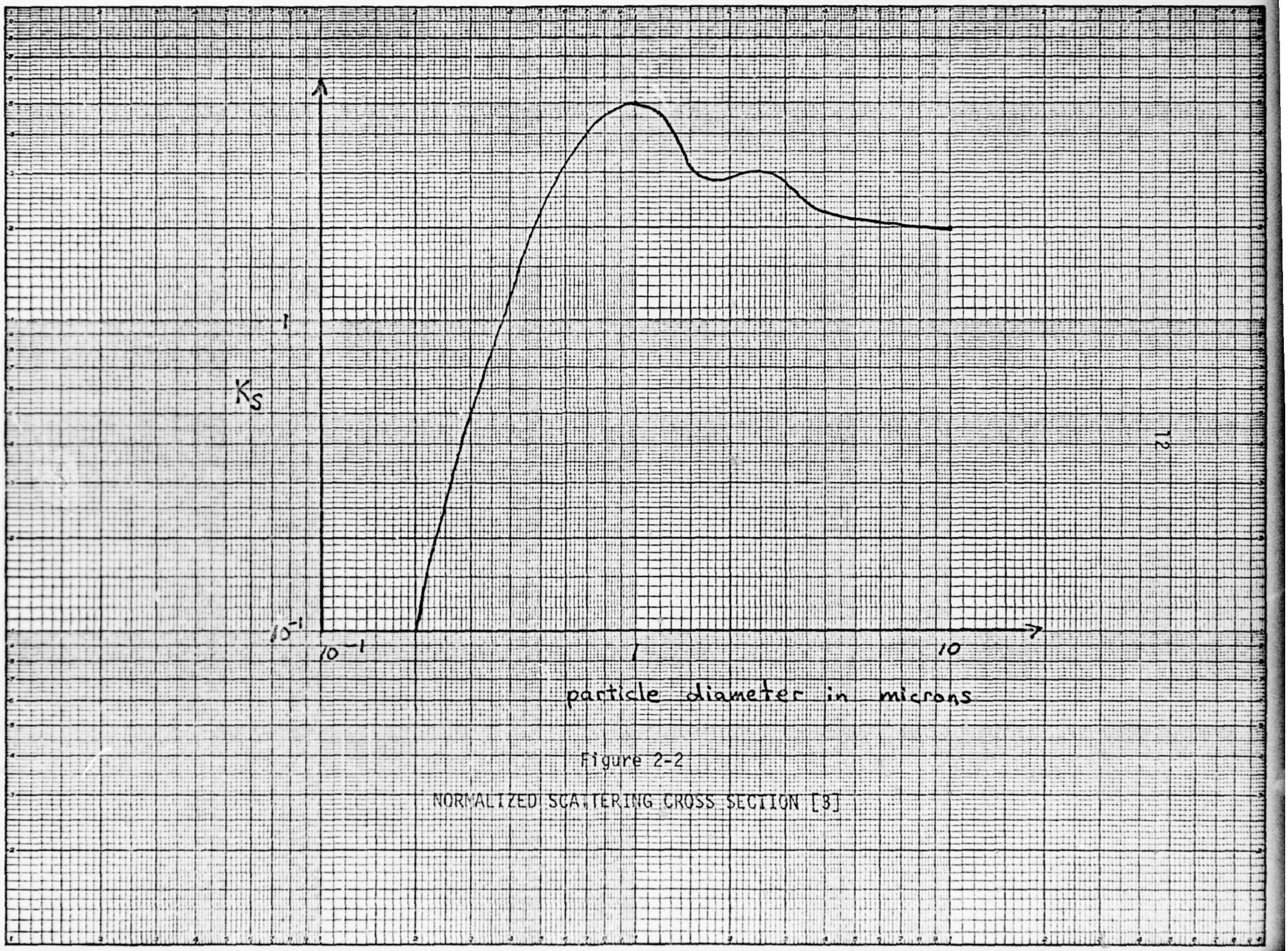

Figure 2-2

NORMALIZED SCATTERING CROSS SECTION [3]

where R_{e_p} = Reynolds number based on particle size

d = Diameter of particle

V_p = Velocity of particle in fluid

ν = Kinematic viscosity of fluid-particle system

The kinematic viscosity has been found to vary with the concentration of particles in the system [8].

$$\alpha = \frac{\Sigma V_o}{V_1} \tag{2.2}$$

where α = Concentration of particles in volume

ΣV_o = Total volume of particles

V_1 = Volume of fluid

For a suspension of rigid particles, the kinematic viscosity is [8],

$$\nu = \frac{5}{2} \alpha \nu_o \tag{2.3}$$

where ν_o = Kinematic viscosity of fluid.

Under conditions where $R_{e_p} < 1$, the inertia terms in the equations of motion are small compared to the fluid friction terms. The equations thus reduce to

$$\text{Mass} \qquad \nabla \cdot \vec{q} = 0 \tag{2.4}$$

$$\text{Momentum} \qquad \vec{q} \cdot \nabla \vec{q} = -\frac{1}{\rho} \nabla p + \frac{\mu}{\rho} \nabla^2 \vec{q} \tag{2.5}$$

where $\vec{q}$ = Mean average velocity of fluid

ρ = Density of fluid

μ = Viscosity of fluid

p = Pressure of fluid.

These equations are solved to determine the flow of particles in the fluid. Reference 7 gives an exhaustive treatment of solutions to these equations under varying conditions.

When solving for accelerated motion of particles, such as flows around bodies or turbulent flows, the lag of the particle behind the fluid velocity becomes important. There is a naturally occurring relaxation time of t', where the particle velocity at t' will be 1/e different from its steady state value. This relaxation time comes out as a coefficient when solving the equations of motion for accelerating flows. It has been shown that for 10 micron particles in air at 20°C, $t' = 1.2 \times 10^{-3}$ sec. [6]. Thus, particles of this size can follow flows with great fidelity up to medium subsonic speeds.

A study by Mazumder and Kirsch [3] using an LDV system showed that particles of .1-2 microns in diameter followed Stokes' law up to turbulent frequencies of 100 kHz in frequency.

2.3 Overall Description of Setup

2.3.1 Complete System

The complete system consisted of the laser and optics, wind tunnel, and photographic system. Figure 2-3 is a diagram of the complete system and Figure 2-4 is a photograph of same.

The laser beam was formed into a sheet of light that passed through the transparent test section of the wind tunnel. Photographs of the flow were made from above the test section. Each segment of the system will now be discussed in detail.

2.3.2 Laser and Optics

A Spectra-Physics Model 166 argon laser was used as the light

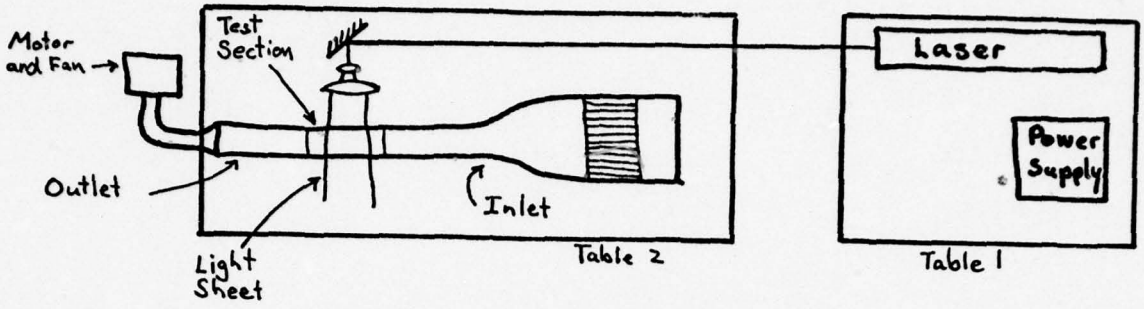

Top View

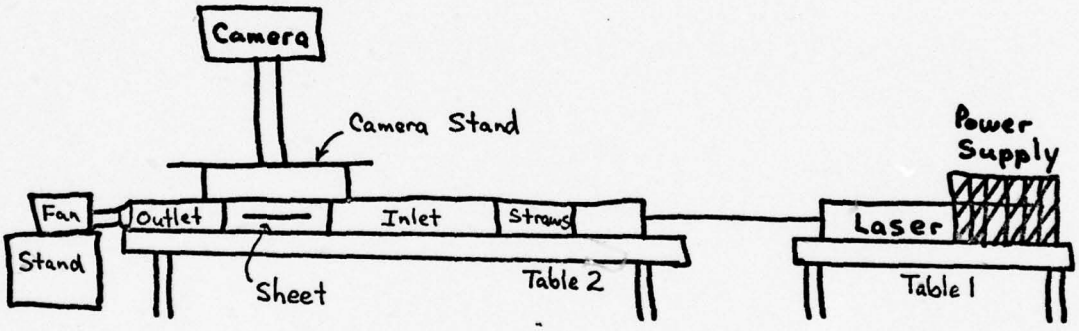

Side View

Figure 2-3

OVERALL LSV SETUP

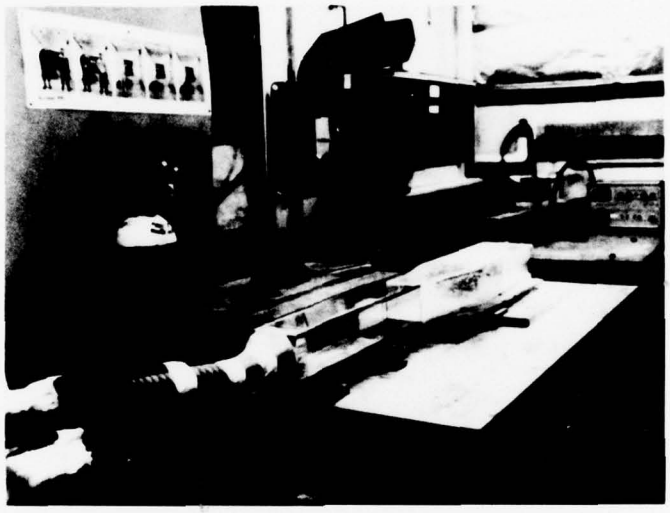

Figure 2-4

OVERALL SETUP

source. It was operated on all lasing lines and gave 3.5 watts output in this mode. A single radial mode was required for the formation of a thin light sheet.

Figure 2-5 is a diagram of the laser and optics used. The laser beam was reflected 90° from a first surface mirror to a 5 mm x 8.5 mm cylindrical lens of 8.2 mm focal length. The cylindrical lens was mounted on an optical rotator to allow precise rotation adjustment of the light sheet. The beam was collimated and focused by a 62 cm, F/5 spherical lens before entering the test section.

Since the laser emits a Gaussian beam, the light sheet has a Gaussian shape, both longitudinally and laterally. Figure 2-6 gives the shape and dimensions of the sheet within the test section.

2.3.3 Wind Tunnel

The wind tunnel was a low speed tunnel built in the laboratory, especially for this research. It consisted of plexiglas inlet and outlet sections, with a glass and plexiglas test section. Figure 2-6 illustrates the shape and dimensions of the wind tunnel.

The inlet contained 0.6 cm diameter plastic straws to collimate the flow and help reduce eddies introduced during particle dispersal. The straws were held in place by the pressure of being packed close together.

No vertical contraction was built into the tunnel due to the complicated cuts and bends that would have been required on the plexiglas. Very little turbulence was noted, even without the vertical contraction. Figure 2-7 is a photograph of the test section, showing the homogeneous, laminar flow.

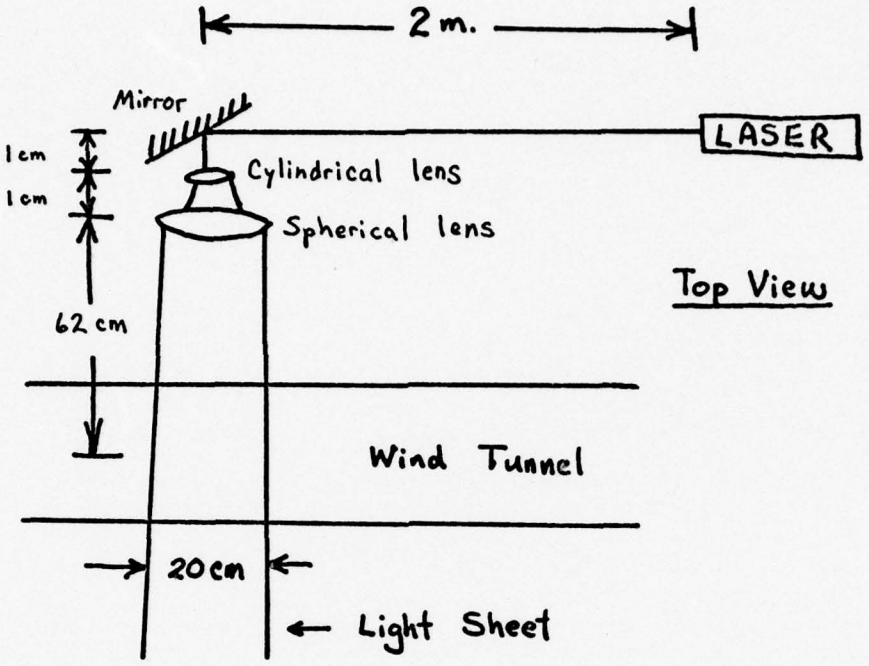

Sheet cross section at tunnel walls

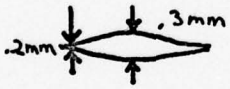

Sheet cross section at tunnel center

Figure 2-5

LASER AND OPTICS

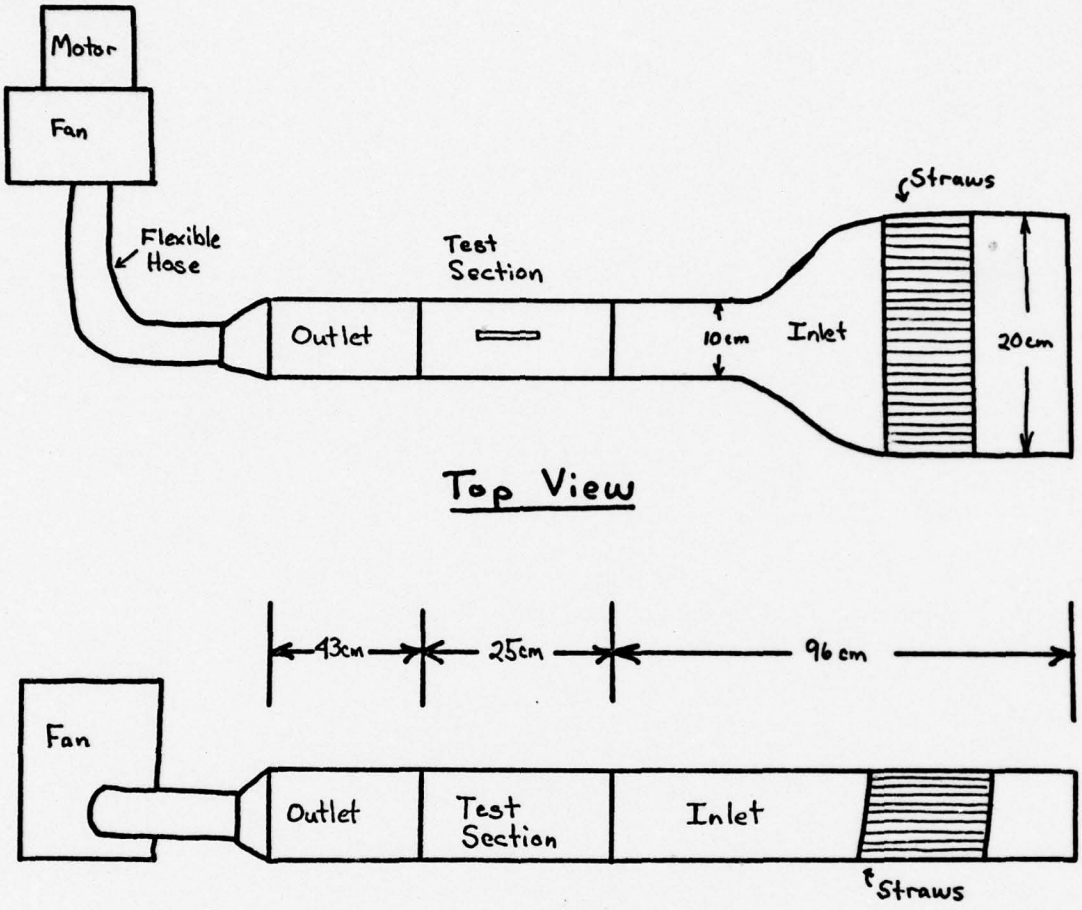

Figure 2-6

WIND TUNNEL

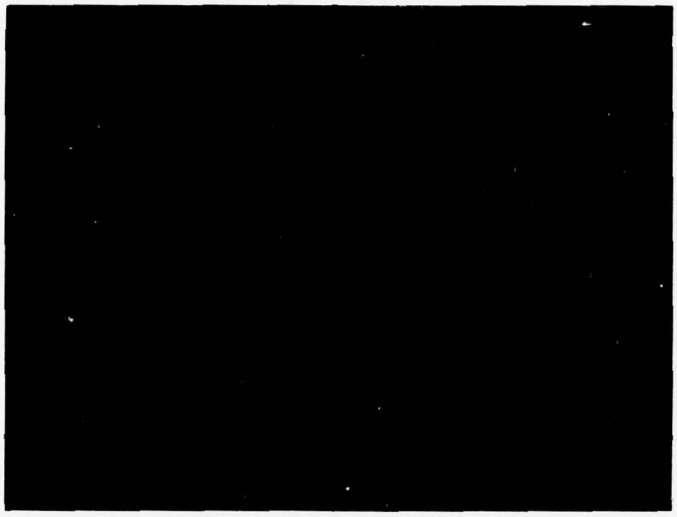

Figure 2-7

FLOW IN WIND TUNNEL

The tunnel was drawn down by a 1/6 hp motor and fan assembly. The outlet was covered with fiberglas air filters to remove most particles from the air. This helped prevent coating of the optics by particulates.

The motor was controlled by a Variac to insure precise control of the airstream velocity in the tunnel.

The wind tunnel and motor were mounted on separate tables to isolate the tunnel from the vibrations of the motor. The laser was mounted on a separate table for the same reason.

The outlet section of the wind tunnel could be disconnected from the test section to allow for insertion and adjustment of the models. The outlet was connected to the fan by a 10 cm flexible hose.

Models were mounted directly into the tunnel or on a sting attached to a translation stage. This allowed precise positioning of the model to within .1 mm.

2.3.4 Photographic System

A Polaroid MP-4 camera system with a 135 mm, F/4.5 Tominon lens, a macro extension, and +1 and +2 closeup lenses were used to make the photographs. The MP-4 was easily adjusted horizontally, vertically, and in angular rotation.

Type 107 Polaroid film of ASA 3000 was used exclusively. This high speed film was needed due to the velocities involved and the amount of light scattered by the particles.

The camera was mounted on a stand that straddled the incoming light sheet. This permitted focusing and framing the photographs from the front of the tunnel assembly.

2.4 LSV System Operation

2.4.1 Introduction

The actual operation of the LSV system involved many problems not readily apparent. The dispersion of particles was critical in getting a uniform coverage of particle streaks on the photograph. Sheet alignment was important to insure a single sheet within the test section. The photographic technique, to include shutter calibration and lens resolution, will also be covered.

2.4.2 Particle Dispersion

The photographic quality was very dependent upon the concentration, size, and dispersion of particles. Water aerosol of approximately 1 micron size was initially used in this research. The aerosol was produced by a Sonicore Model 035 H nozzle. This nozzle was unsatisfactory with this setup because the nozzle produced too many particles for the size of the tunnel. It also introduced a high degree of turbulence to the flow. The water particles were weak light scatterers, while the high water vapor content caused blooming on the photographs at power settings over 2 watts. This washed out streaks from individual particles.

Solid particles such as chalk dust, alumina particles, and talc were tried in the tunnel. The talc was the easiest to disperse into the tunnel as well as being the most efficient light scatterer. The talc particles ranged in size up to 20 microns, with a mean of 10 microns. No effort was made in this research to make the particles smaller or of uniform size. Johnson's Baby Powder was the type of talc used.

The change to solid particles required a different dispersion

technique from the nozzle used previously. A thin plate vibrator was built to shake off the particles at high frequency into the flow. It was so noisy and introduced so much turbulence into the flow that it was discarded.

The technique that worked best was manually squeezing the plastic talc bottle to inject the proper number of particles into the flow. The bottle was shaken up to loosen the particles and then gently squeezed near the tunnel entrance. This produced clouds of particles with little velocity of their own. These clouds would mix throughout the tunnel to give a homogeneous dispersion in the test section. The particles could be injected and a picture taken by the same person with the aid of a cable release on the camera.

2.4.3 Sheet Alignment

The wind tunnel was raised with aluminum plates until the center of the test section was level with the output of the laser. The test section was precisely adjusted with shims to eliminate angular reflections of the sheet back into the test section. This was imperative to insure a single thin sheet in the test section. The procedure was repeated when the orientation of the sheet was changed.

2.4.4 Photographic Technique

The photography of a model began with the correct orientation of the sheet and model for the information desired. The correct concentration of particles was required for a meaningful photograph. Too few particles and the general shape of the flow could not be seen and too many would cause the streaks to run together. Trial and error was the only way to initially arrive at the proper concentration.

The camera shutter speed was adjusted to give a 3-6 mm streak length for the characteristic flow being measured. Frequently, two exposures of the same area were required if there were adjacent areas of high and low speed flows.

The depth of field was sometimes a problem, as when photographing with the sheet near the vertical position. In this case, the aperture was stopped down as much as possible to increase the depth of field.

Accurate focusing was always a problem, since at F/4.5 the depth of field was only 1 mm. The camera was focused on an object placed in the sheet or on the model itself if it protruded the sheet. The ground glass focusing screen on the MP-4 was extremely useful in this respect.

The camera and stand were steadied before each photograph since the height of the column allowed some camera movement, particularly when the film was pulled from the camera.

2.4.5 Shutter Calibration

Since the velocity measurements depend upon accurately knowing the shutter speeds, the shutter was calibrated on an oscilloscope. The calibration setup and shutter speeds are shown in Figure 2-8. Five measurements were made at each shutter speed to arrive at the average error.

2.4.6 Lens Resolution

Tests were made at each aperture setting to determine the maximum resolution. The results are shown below.

F/4.5 = 8 lines/mm F/8 = 11 lines/mm

F/5.6 = 11 lines/mm F/11 = 11 lines/mm

F/16 = 11 lines/mm

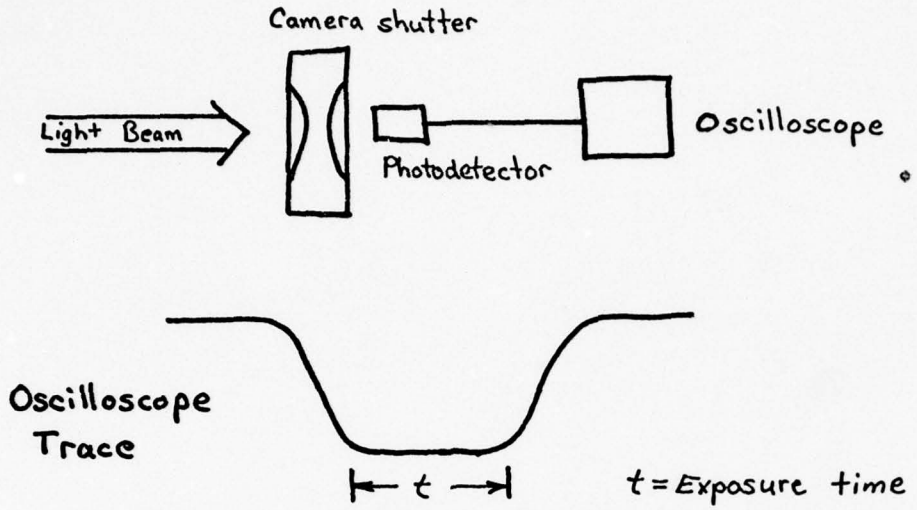

$\frac{1}{400}$ = 2.8 msec $\pm$ 1%

$\frac{1}{250}$ = 4.15 msec $\pm$ .5%

$\frac{1}{125}$ = 7.8 msec $\pm$ .3%

$\frac{1}{60}$ = 15.5 msec $\pm$ .1%

$\frac{1}{30}$ = 25.4 msec $\pm$ 11%

$\frac{1}{15}$ = 52.5 msec $\pm$ 4%

$\frac{1}{8}$ = 100.5 msec $\pm$ 4%

$\frac{1}{4}$ = 204.4 msec $\pm$ 2%

$\frac{1}{2}$ = 415.0 msec $\pm$ 1%

1 = 837.5 msec $\pm$ 1%

Figure 2-8

SHUTTER CALIBRATION

A test chart was mounted on a sting to check the resolution with the tunnel off and on. No noticeable difference could be noted.

The maximum resolution of 11 lines/mm indicates that the 10 micron particles left streaks approximately 100 microns thick on the film.

Chapter 3

MEASUREMENT OF VELOCITIES IN A BOUNDARY LAYER ON A FLAT PLATE

3.1 Introduction

The study of boundary layers in aeronautics is of major importance. Characteristics such as lift and drag on a body are influenced greatly by mechanisms that occur within the boundary layer. Precise measurement of velocities within the boundary layer are important in understanding how the fluid reacts to bodies.

The boundary layer on the top of a thin flat plate was measured with LSV. The data measured and comparison of results with theory are discussed.

3.2 *Experimental Setup and Procedure*

Figure 3-1 shows the setup for measuring the boundary layer velocities on a 10x15 cm flat plate. The plate was made of .010 inch stainless steel and coated with Teflon spray to smooth the surface. It was mounted on a 10 cm sting made of welding rod. The plate was mounted in the tunnel parallel to the free stream flow and controlled vertically by the translation stage holding the sting.

The light sheet was horizontal and parallel to the top of the flat plate. Alignment of the sheet and flat plate were critical to insure that they were parallel. This was done with the translation stage at its maximum extension and the sheet grazing the top of the flat plate at zero depth. The depth of the measurements taken could then be read off of the dial on the translation stage as the flat plate was lowered in relation to the light sheet.

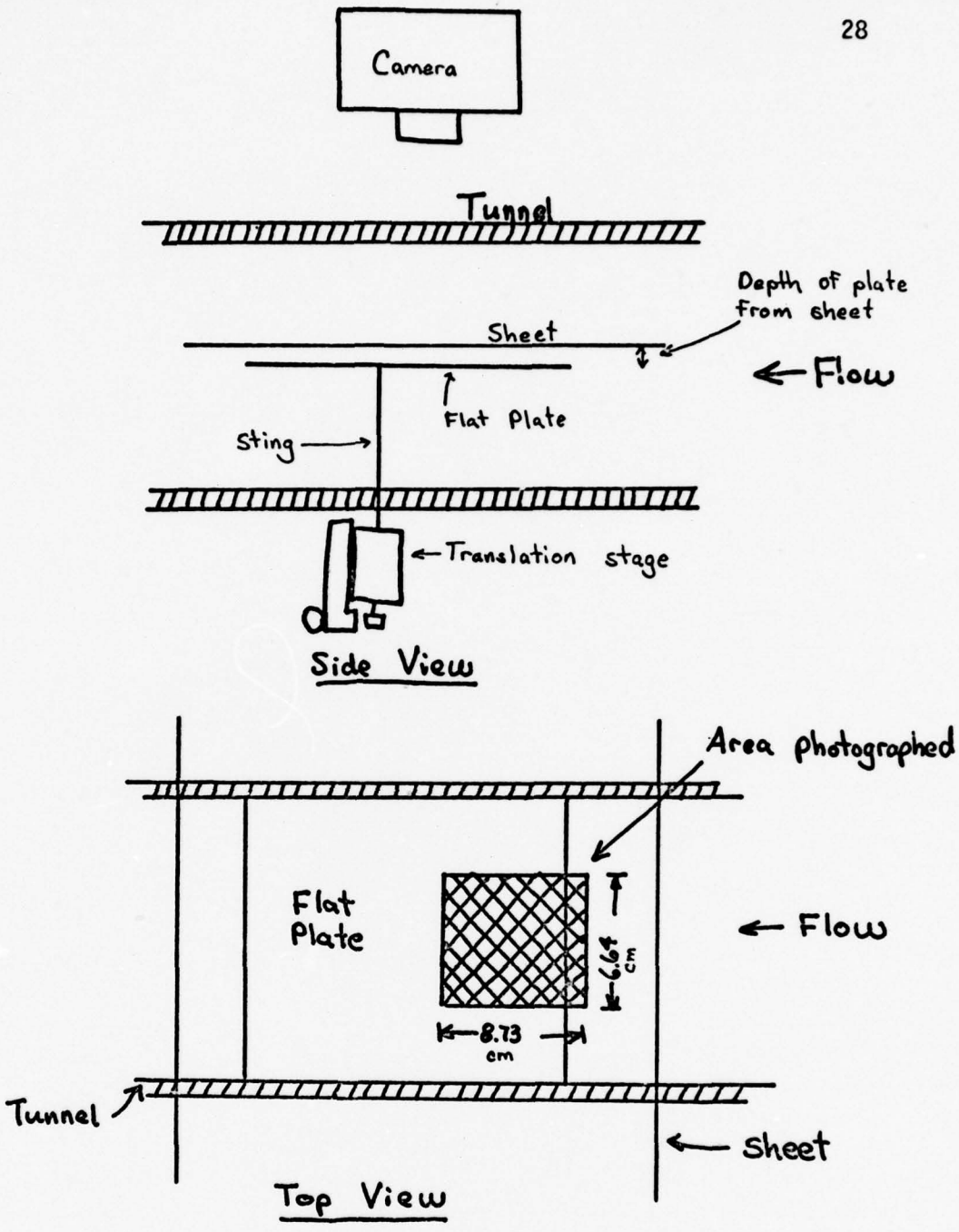

Figure 3-1

SETUP FOR FLAT PLATE BOUNDARY LAYER MEASUREMENTS

The camera was located directly above the flat plate and perpendicular to the sheet. A magnification of 1.1 was used to look at the central part of the flat plate immediately behind the leading edge, as shown in Figure 10. This area was chosen to reduce the effects of the tunnel walls and the trailing edge of the finite flat plate.

Exposures were made every .2 mm, beginning at .2 mm depth. Shutter speeds were 1/15, 1/30, and 1/60 second at apertures of F/16 to F/5.6.

3.3 Data Reduction and Results

The streak lengths could be measured directly from the photographs or transferred to transparencies for projection onto a screen for measurement. The measurements taken in this thesis were taken directly from the photographs.

Since there are minor streak length variations over the same area, the measurement of lengths is somewhat subjective. The error uncertainty stated in the data was arrived at through measurements of the same area by different people.

Figures 3-2 to 3-5 are representative photographs taken on the flat plate. Figure 3-2A is taken at .2 mm from the plate surface. It is noticed that there are large variations in streak length over the same area. These are caused by the inertia of some particles causing them to be deposited on the plate's surface. Large slow particles are also seen as shortened streaks. The velocity change as the particles progress downstream can be clearly recognized by the progressive shortening of the streaks in the x-direction.

A polaroid was used in front of the lens for Figure 3-2A to reduce

A

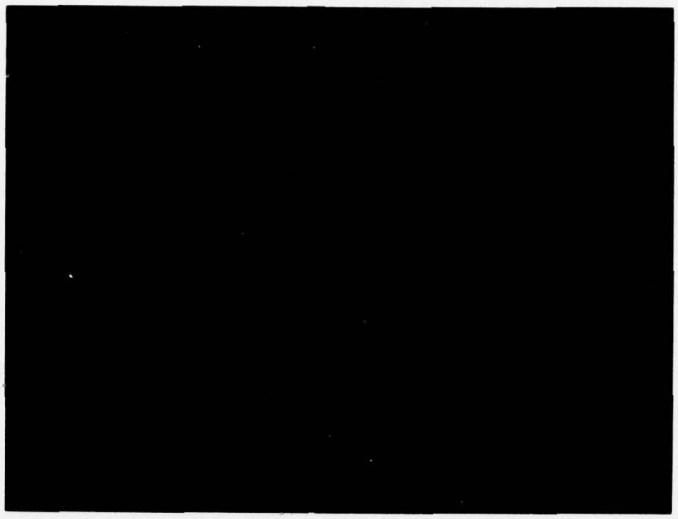

Depth = .2 mm Exposure Time = 52.5 msec

B

Depth = .6 mm Exposure Time = 25.4 msec

Figure 3-2

MEASUREMENTS IN A BOUNDARY LAYER

A

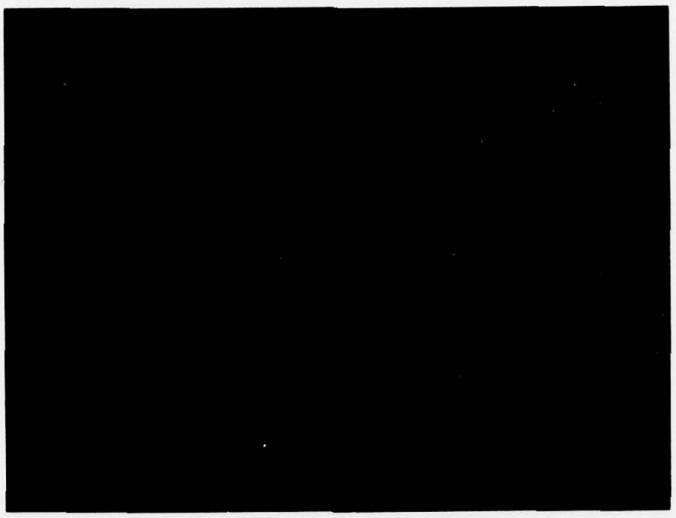

Depth = 1 mm Exposure Time = 25.4 msec

B

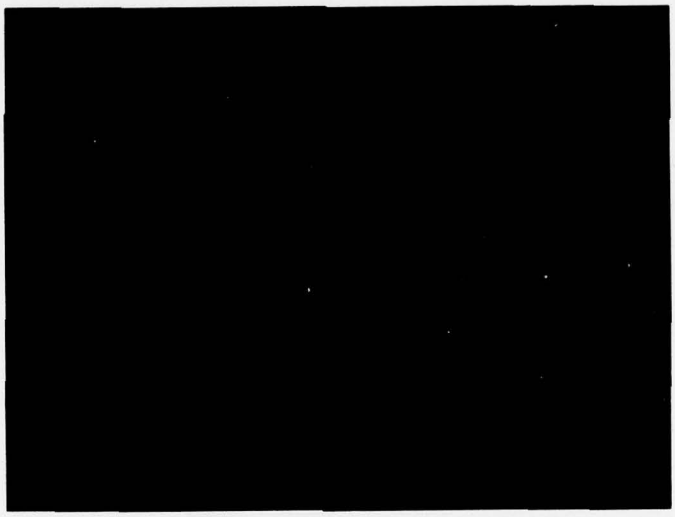

Depth = 2 mm Exposure Time = 15.5 msec

Figure 3-3

MEASUREMENTS IN A BOUNDARY LAYER

A

Depth = 3 mm Exposure Time = 15.5 msec

B

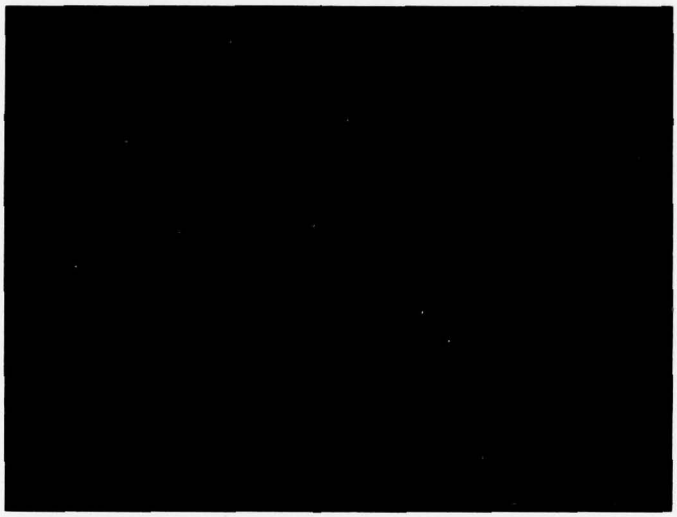

Depth = 4 mm Exposure Time = 15.5 msec

Figure 3-4

MEASUREMENTS IN A BOUNDARY LAYER

A

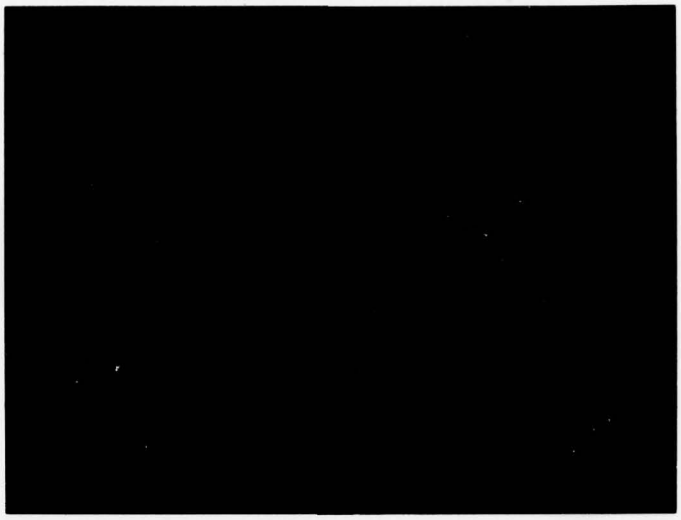

Depth = 5 mm

Exposure Time = 15.5 msec

B

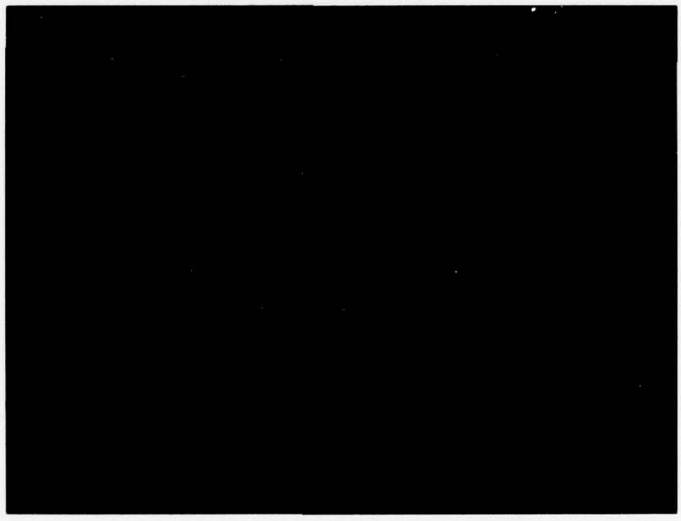

Free Stream Velocity

Exposure Time = 15.5 msec

Figure 3-5

MEASUREMENTS IN BOUNDARY LAYER

the glare of the light sheet from the surface of the plate. The plate reflected the laser light without appreciably changing the polarization, while the particles scattered light in all directions, destroying the polarization. Thus, the glare can be cut out while passing the light from the particles.

The two dimensionality of the flow was checked by doubling the exposure time and confirming that the streak length doubled.

Measurements of streak length were made 2.76 cm from the leading edge of the flat plate and across the entire area covered by the photograph. This distance was chosen because that is where the boundary layer should be .5 cm thick, the maximum extension on the translation stage. The free stream velocity, Figure 3-5B, was measured initially to determine that point.

Each photograph was measured over the designated area. The maximum, medium and minimum streak lengths were used to find the velocities. These velocities are plotted in Figure 3-6. The distribution of particle lengths was skewed toward the maximum value, with over 70% being greater than medium in length.

3.4 Comparison of Results with Theory

Figure 3-6 is the graph of the ratio of boundary layer velocity to free stream velocity plotted against η.

$$\eta = y\sqrt{\frac{U_\infty}{\nu x}} \tag{3.1}$$

where η = Dimensionless coordinate

y = Perpendicular distance from surface of plate

U_∞ = Free stream velocity

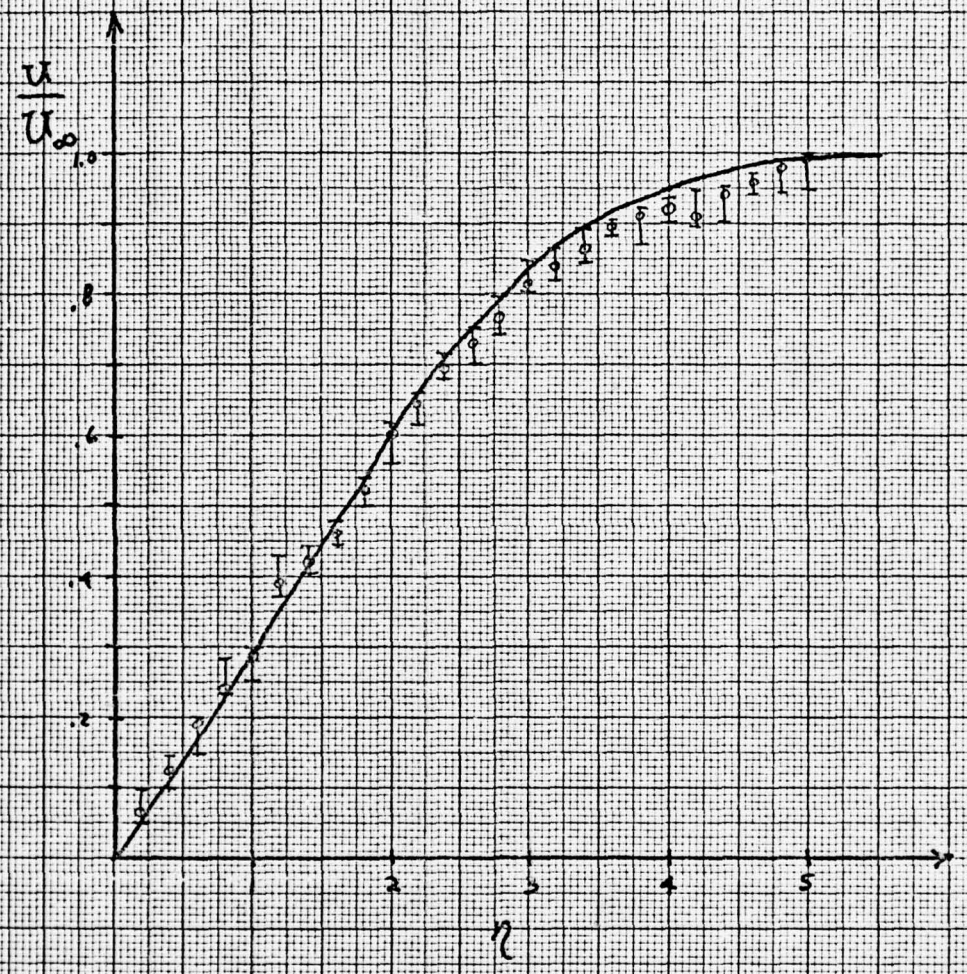

Figure 3-6

VELOCITY IN BOUNDARY LAYER OF FLAT PLATE

ν = Kinematic viscosity of fluid

x = Distance downstream from leading edge

The solid line is the theoretical curve of the velocity in a boundary layer on a flat plate as predicted by Blasius [10]. Also plotted are experimental results by Nikuradse [10].

The point of measurement downstream was determined by the maximum extension of the translation stage, .5 cm. The boundary layer thickness, δ, is defined as the point where the velocity is 99% of the free stream velocity. According to Blasius [10],

$$\delta \cong 5\sqrt{\frac{\nu x}{U_\infty}} \tag{3.2}$$

Solving for δ = .5 cm with U_∞ = 36.36cm/sec gives an x of 2.51 cm. But since the picture is taken with 1.1 magnification, this relates to 2.76 cm from the leading edge on the photograph.

It is seen in Figure 3-6 that the largest deviations from the theoretical curve occur near the surface of the plate. This is primarily due to deposition of the particles on the surface of the plate and to the finite thickness of the sheet in an area of large velocity changes with small depth changes. The errors involved vary from 52% at .2 mm depth to 4% at 5 mm depth, with an average of 10%.

When only the maximum streak lengths were used, the deviation from the theoretical curve was considerably less. This was to be expected since there are no mechanisms to make the particles go faster than the local fluid, but particle inertia and particles exiting the sheet can cause shortening of the streaks. When the maximum streaks were used, the deviation from theory went from 52% at .2 mm to 1% at 5 mm. The average in this case was only 4%.

Tests were conducted on several people to determine the uncertainty in the measurements of streak lengths. An uncertainty of 5% was found for all measurements discussed in this thesis.

3.5 Conclusion

It has been shown that the streak technique is an accurate method of measuring the velocities in a low speed boundary layer on a flat plate. The accuracy of these measurements is most affected by particle deposition and the finite thickness of the light sheet, particularly when making measurements near the plate surface. The measurements taken agreed well with theory, especially when the maximum streak lengths over an area were used.

Chapter 4

MEASUREMENT OF FLOW PAST A CIRCULAR CYLINDER

4.1 Introduction

Two-dimensional flow past a circular cylinder has been of interest since the science of fluid mechanics began. It is a basic shape which has been extensively studied, but still has not been solved analytically for flows with Reynolds numbers over 100 because the flow goes unsteady [14]. The wake behind a circular cylinder was measured for low Reynolds numbers. Where possible, these results are compared to existing theory or previous experimental results.

4.2 Experimental Setup and Procedure

Figure 4-1 is a diagram of the setup for making measurements on a circular cylinder. The cylinder was 10 cm long, 1.6 cm in diameter, with a length/diameter ratio of 6.25. The cylinder was held in the tunnel with beeswax.

The light sheet was horizontal and parallel to the free stream flow. Since the cylinder cut the sheet, a bright ring could be seen on the cylinder. To reduce the glare of this ring on the photographs, the cylinder was painted a dark purple to absorb the light.

The shadow of the sheet behind the cylinder was reduced by reflecting part of the sheet back into the tunnel with a first surface mirror mounted on an adjustable mirror mount. Precise adjustment of the secondary mirror was necessary to keep the reflection in the plane of the original sheet. The secondary reflection caused some areas to receive double illumination. This showed up in the photographs as sectioned dark and light areas in the

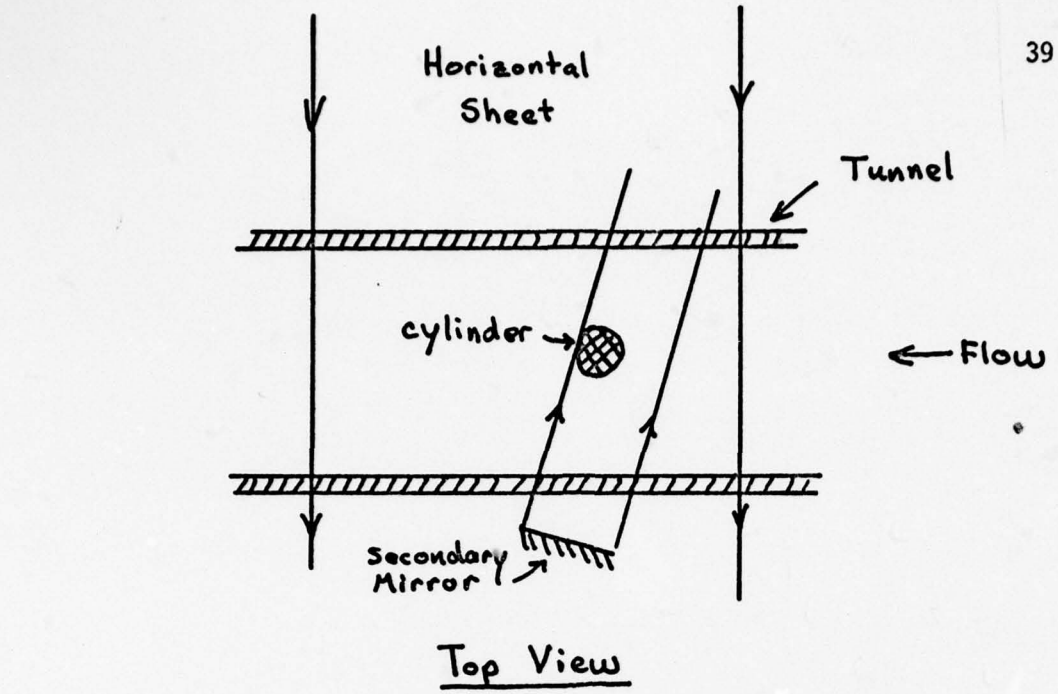

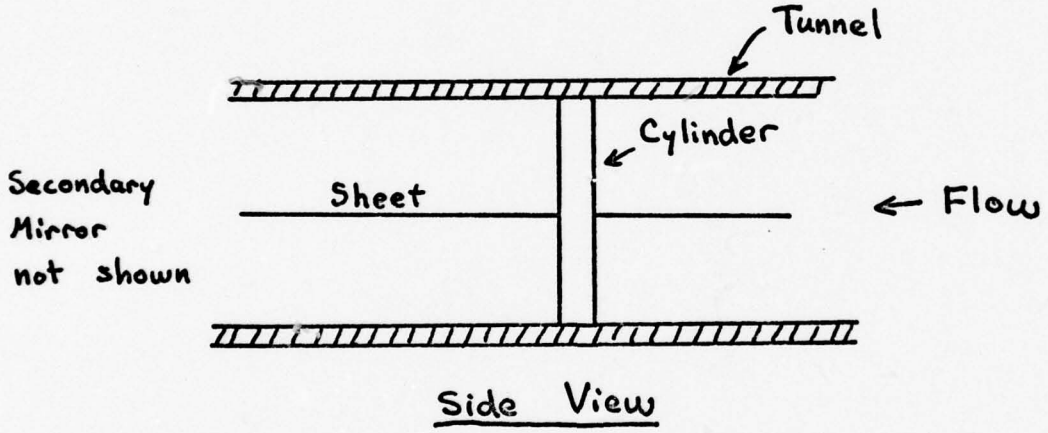

Figure 4-1

SETUP FOR FLOW AROUND CIRCULAR CYLINDER

flow.

4.3 Results

Figure 4-2 is a photograph of the wake behind a circular cylinder for a Reynolds number of 75.6. It should be noted that the length of the wake is a subjective measurement since it is not readily apparent where the streamlines rejoin. Measurements made on wake lengths for several different Reynolds numbers are plotted in Figure 4-3.

There are two high speed chutes on the top and bottom of the wake. These are caused by the acceleration of the flow around the cylinder. They are readily seen in Figure 4-2.

There are also two symmetrical eddies that are recognizable immediately behind the cylinder in Figure 4-2. Figure 4-4 is an enlargement of the eddies. The circulation around two central cores and the velocity gradients moving away from the core centers are both evident in this photograph.

The streak lengths in Figure 4-4A were measured and the velocity field mapped out in Figure 4-4B. Representative streak lengths in small areas were measured to arrive at the mapping.

Figure 4-5 is a photograph of the immediate wake behind a circular cylinder during the formation of a Karman vortex street. The same procedure as above was used to map the velocities for Figure 4-5B.

Figure 4-6 is an enlarged photograph of the separation point on a circular cylinder at a Reynolds number of 300. Several different photographs at Re = 300 were measured to find the angle of separation of the flow from the forward stagnation point. The average angle of separation was

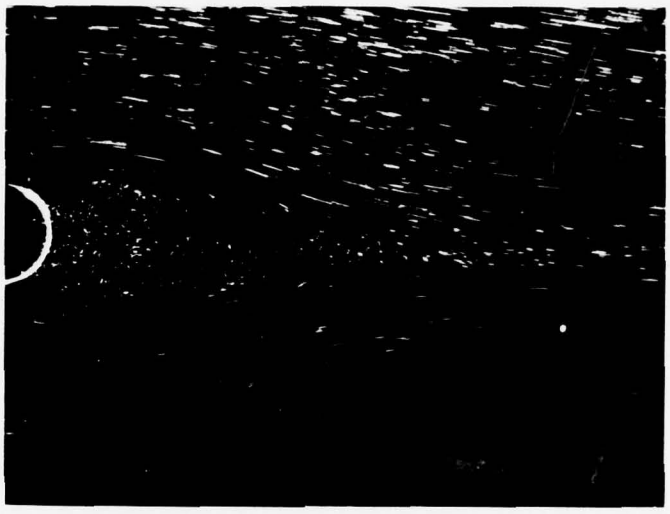

Re = 75.6 Exposure Time = 100.5 msec

Figure 4-2

WAKE LENGTH BEHIND CIRCULAR CYLINDER

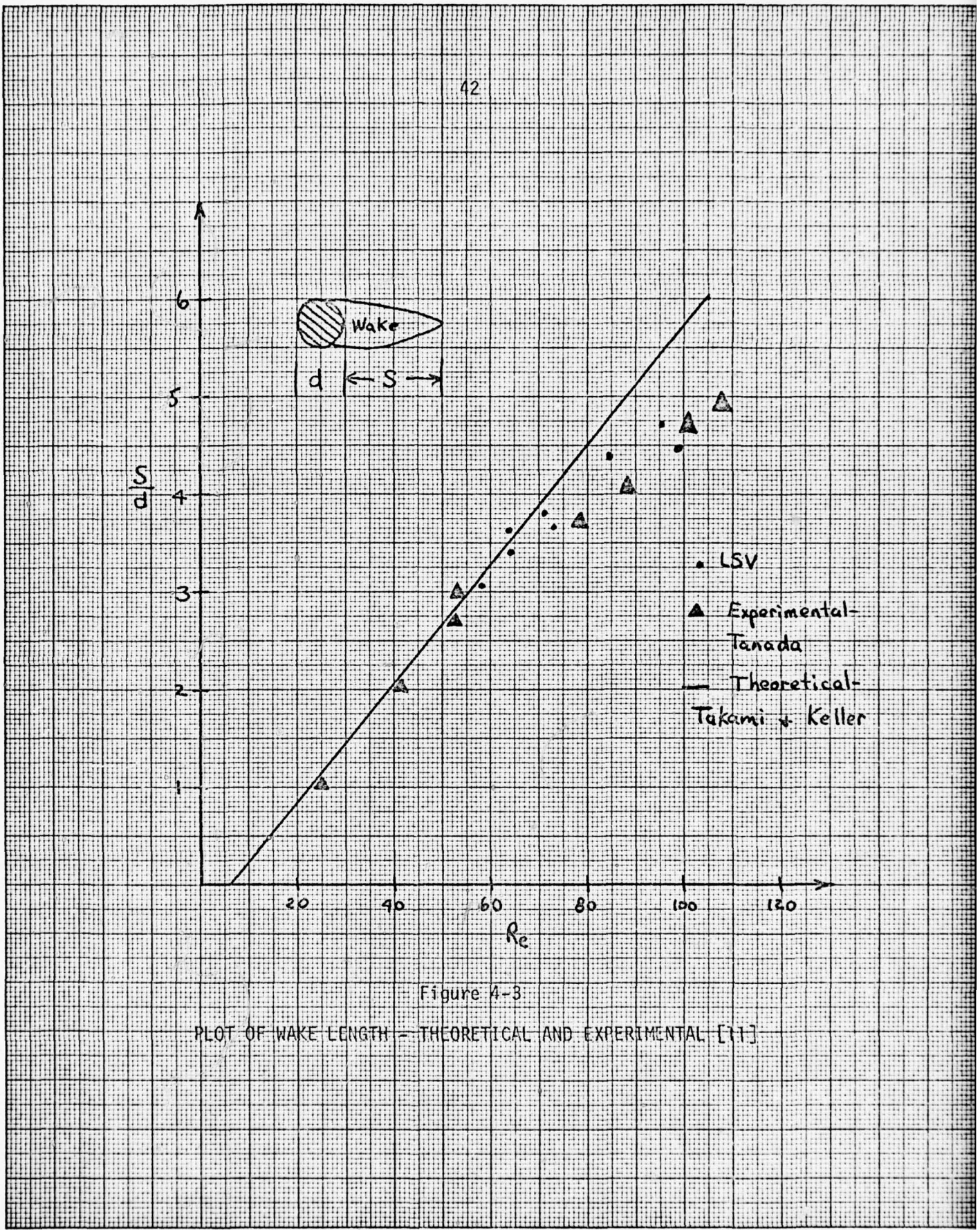

Figure 4-3

PLOT OF WAKE LENGTH – THEORETICAL AND EXPERIMENTAL [11]

A

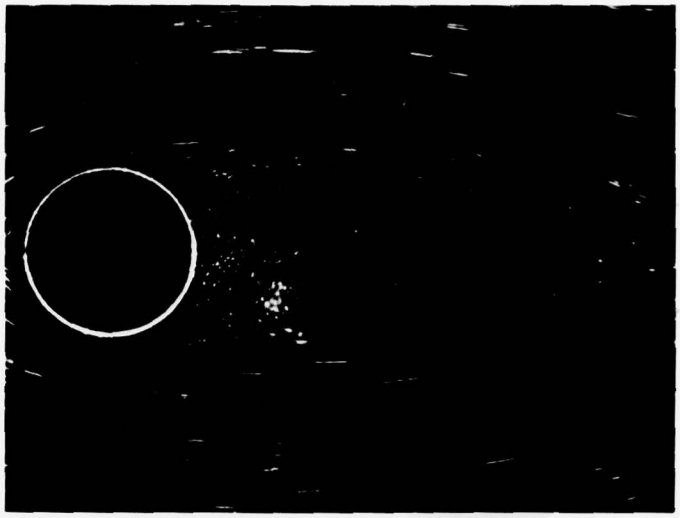

Re = 90 Exposure time = 52.5 msec

B

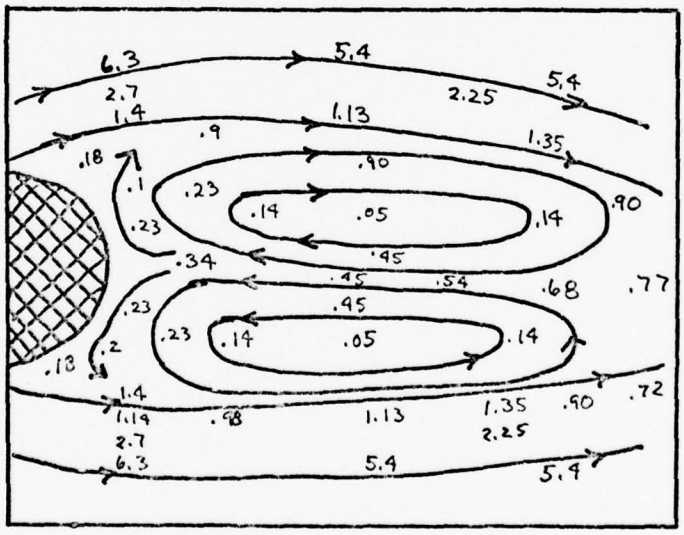

Velocities in cm/sec

Figure 4-4

EDDIES BEHIND CIRCULAR CYLINDER

A

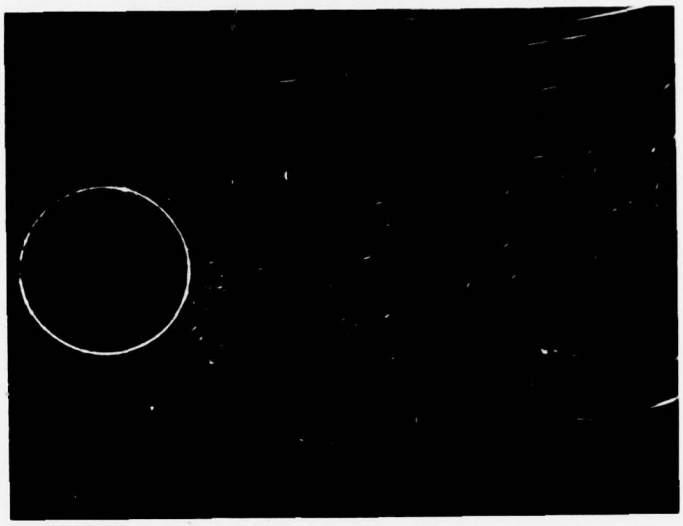

Re = 270 Exposure time = 25.4 msec

B

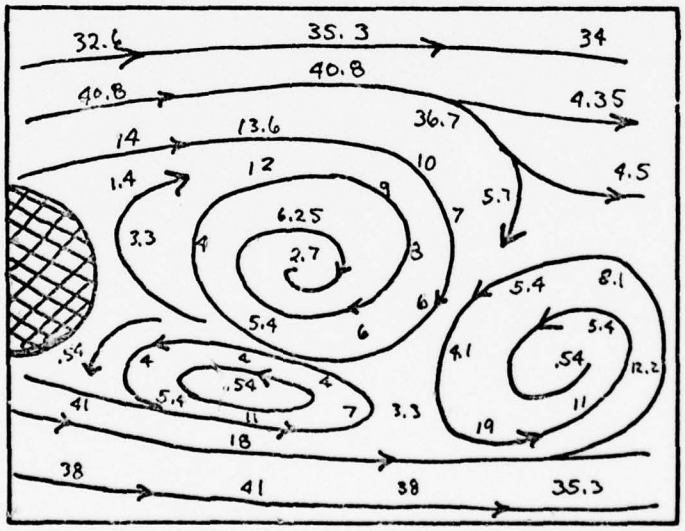

Figure 4-5

VORTEX SHEDDING BEHIND CIRCULAR CYLINDER

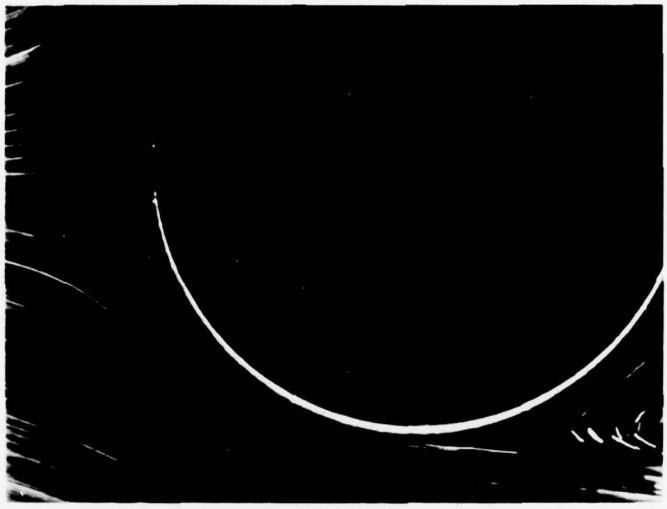

Re = 300 Exposure Time = 52.5 msec

Figure 4-6

SEPARATION POINT ON CIRCULAR CYLINDER

81.5° ± 1.5°.

4.4 Comparison of Results with Theory

4.4.1 Review of Theory

The flow around a circular cylinder changes dramatically as the Reynolds number increases. A brief review of the theory of the flow as the Reynolds number increases will make comparison of results and theory more understandable.

As the fluid moves around the walls of the cylinder, vorticity is created by the velocity difference between the body and the adjoining fluid. At Reynolds numbers below about 6, the negative vorticity from the top of the cylinder and the positive vorticity from the bottom are swept to the rear of the cylinder in the boundary layer. At Re = 6, there is just enough vorticity at the rear of the cylinder to satisfy the no-slip condition. This causes a forward flow to develop, reflecting the rearward moving fluid away from the cylinder. The end result is the formation of two symmetric eddies behind the cylinder [8].

As the Reynolds number increases, the wake containing the two eddies grows in length. Far downstream, the wake becomes unstable and begins to oscillate in an almost sinusoidal fashion.

As the Reynolds number increases further, the oscillations grow until the eddies begin to shed downstream, alternately from one side and then the other. This critical Reynolds number for shedding is a function of the cylinder length/diameter. In the case of the cylinder used here, it was Re = 120.

The shed vortices form a Karman vortex street behind the cylinder.

They are concentrated packets of opposite vorticity spaced alternately on opposing sides of the wake at definite intervals depending upon the Reynolds number [12]. The street is recognizable beyond 4-5 diameters downstream of the cylinder and can be seen up to Re ≅ 2500. However, definite periodic oscillations occur up to Re = 4×10^5 but the vortices are not recognizable downstream due to mixing [8]. Above this Reynolds number, the boundary layer becomes turbulent and the oscillations cease.

4.4.2 Visualization Measurements

Figure 4-3 is a graph of wake length versus Reynolds number. The experimental results of this thesis are plotted along with the theoretical curve according to Takami and Keller [11] and Tanada's experimental results [14]. The streak technique gave results that compared well with theory up to Re = 75 but began to fall off after that point. A similar result was obtained by Tanada and others. The length of the wake is a subjective measurement and may account for the deviation at high Reynolds number. Figure 4-2 illustrates that the point where the streamlines rejoin is not definite.

A vortex street was not found to form before a Reynolds number of around 150 in this experiment. This is in contrast to Re ≅ 120 that the theory predicts. The tunnel walls may have delayed shedding for some time.

Hiemenz predicted that the angle of separation of the flow during the formation of a vortex street is 82°. He confirmed this by experiment [13]. This thesis is in excellent agreement on this point, as shown in Figure 4-6. The angle measured here was 81.5° ± 1.5°.

4.4.3 Velocity Measurements

Figure 4-7 is a plot of the velocity across the wake 1.1 diameters downstream from the cylinder. The data points were taken from the velocity mapping of Figure 4-4. Also plotted are measurements taken by Nishioka with a hot wire [11]. He stated that the velocity should go to zero in the eddies, but that the unsteadiness of the eddies and the low resolution of the hot wire caused errors in his results. The streak technique is more accurate in this respect since it made an instantaneous record of the velocities in the eddies. The graph nearly reaches zero velocity at the positions of the eddy centers.

There are no previous results to compare with the vortex shedding of Figure 4-5. This is because the flow is highly unsteady, making previous velocity measuring techniques impractical.

4.5 Conclusion

The streak technique has been shown to agree well with theory and previous experiments of flow past a circular cylinder, both as a visualization technique and for velocity mapping. The new technique is capable of measuring instantaneous velocities in unsteady flows such as the shedding vortices of the Karman vortex street. This technique should prove very valuable in studying flows of this type.

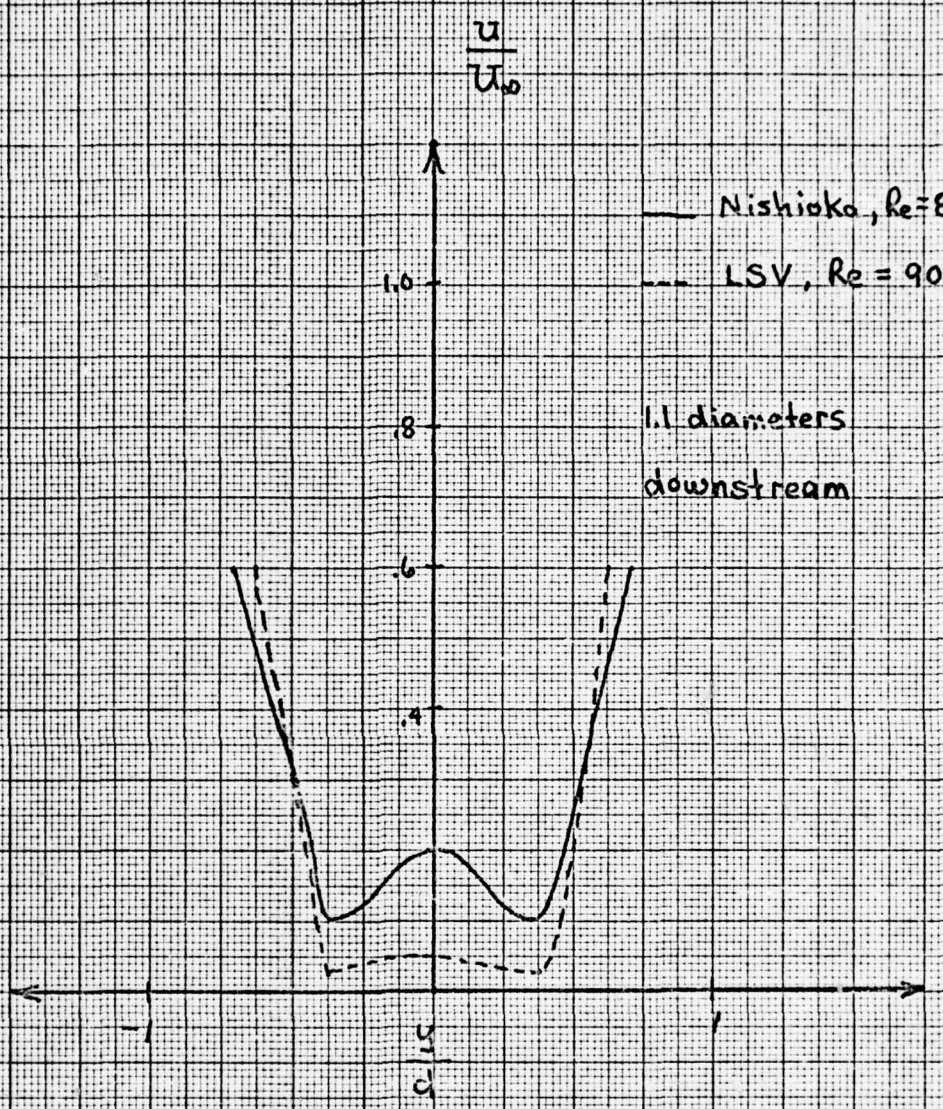

Figure 4-7

VELOCITY PROFILE ACROSS WAKE OF CIRCULAR CYLINDER

Chapter 5

MEASUREMENT OF THE FLOW OVER A DELTA WING

5.1 Introduction

Supersonic flight brought forth many new dimensions in aeronautics. Among these was the delta wing, a highly swept, low aspect ratio wing used on such high performance aircraft as the F-106. The high speed characteristics of such wings generated much interest and research. However, any high speed aircraft must operate in the low speed regime during takeoff and landing. The low speed characteristics are thus very important in the design of any delta wing.

Previous experimental research on delta wings involved static pressure measurements on the wing surface, pressure measurements within the vortex cores by pressure tubes, and boundary layer visualization with a paraffin and chalk mixture [17]. The static pressure measurements on the wing surface and the boundary layer visualization gave only local conditions on the surface. The pressure tubes that were used to measure the pressure head of the vortices undoubtedly disturbed the flow.

Smoke and tufts on wires have been used to determine the size and location of the vortices on the delta wing [18]. Such methods give little quantitative information on the velocities above the wing. These methods are commonly used for current low speed research.

The laser streak velocimetry technique was used to analyze the flow over the top of a delta wing. The results of measurements and comparison with known theory is presented in this chapter.

5.2 Experimental Setup and Procedure

The overall setup for measuring the velocities on a delta wing is shown in Figure 5-1. The wing model was made of .020 inch aluminum and had a sweepback angle of 60°. The edges had double bevels as shown in Figure 5-2. The surface of the model was coated with Teflon spray to fill in minor imperfections in the surface.

The initial angle of attack was set on the sheet and the model aligned on it. Photographs were made at .2 mm intervals up to 5 mm from the surface of the plate at 5°, 15° and 25° angle of attack.

An alternate setup was used to measure the two dimensionality of the flow in a central core, as shown in Figure 5-3. The wing was mounted parallel to the sting so that the camera had an edge view of the model instead of a planform view as before. The light sheet was set parallel to the free stream flow and level with the centerline of the model. Photographs were made at 5°, 15° and 25° angle of attack.

All photographs were made at a constant tunnel velocity of 101 $\frac{cm}{sec}$ or Re = 3570, based on the chord of the delta wing. A shutter speed of 7.8 msec was used on all photographs.

5.3 Data Analysis

A brief review of the theory of flow over the top of a delta wing is in order before discussing the data. A wing shape is normally chosen to allow a small angle of attack at cruise airspeeds. During takeoff and landing, a larger angle of attack is thus required because of the reduced airspeed. Boundary layer separation on the top of a delta wing occurs at small angles of attack. During low speed operation, viscous forces in the

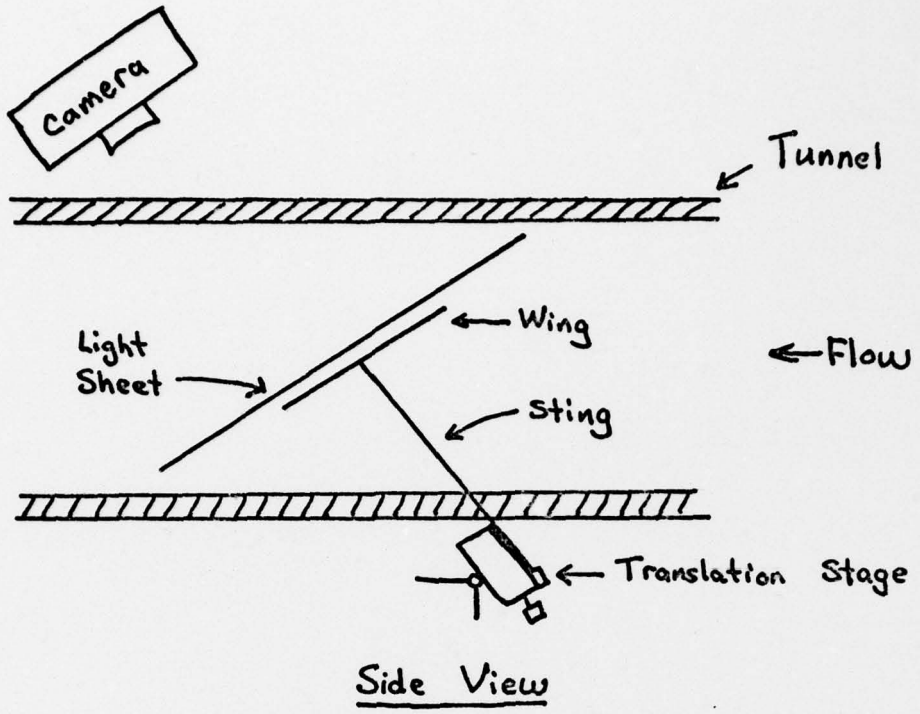

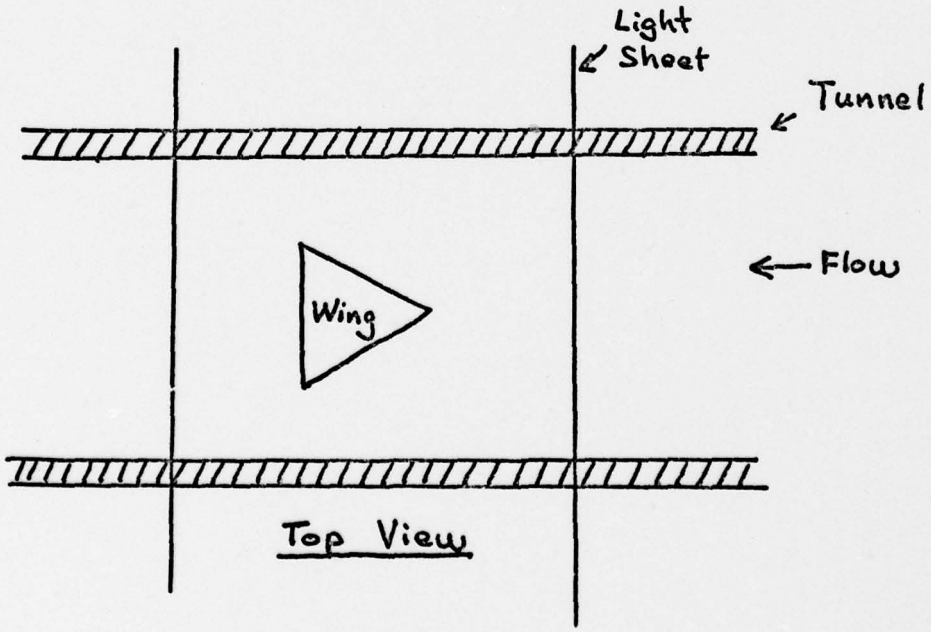

Figure 5-1

SETUP FOR MEASUREMENTS ON DELTA WING

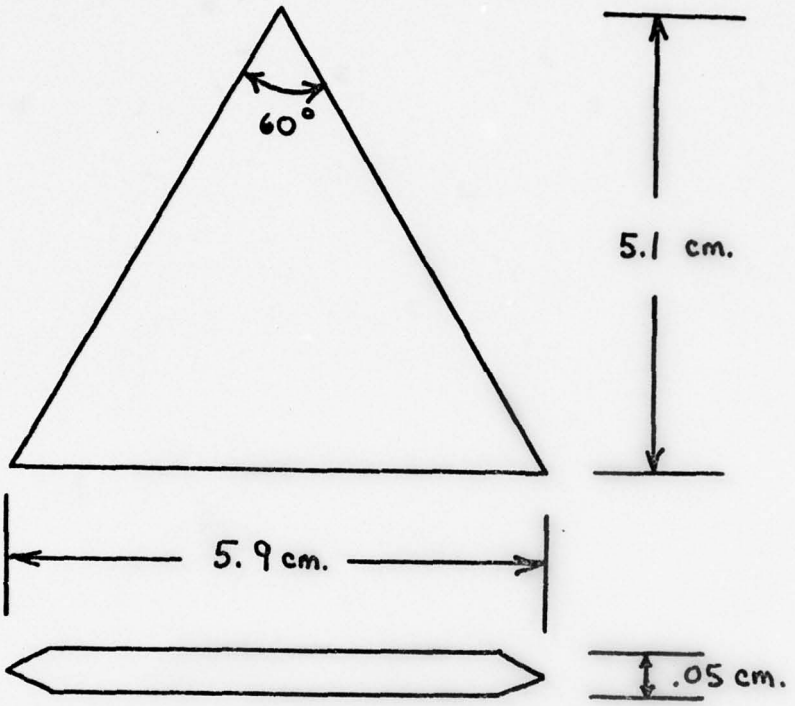

Figure 5-2

DELTA WING MODEL

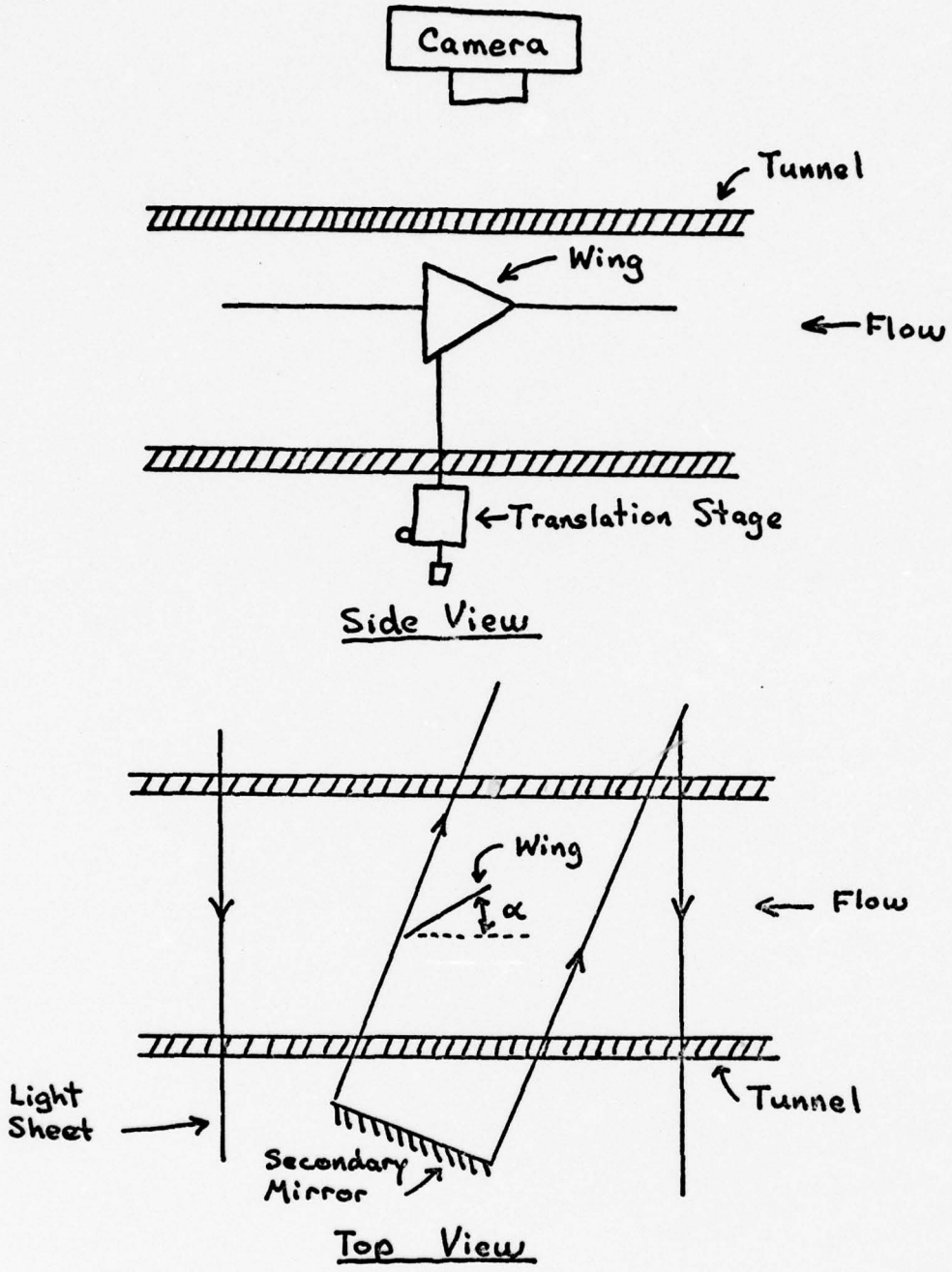

Figure 5-3

ALTERNATE SETUP FOR MEASUREMENTS ON DELTA WING

boundary layer cause separation at the leading edges [19]. A sheet of vorticity, most of which is in the streamwise direction, is shed from each leading edge. These sheets roll up into two tornado-like spirals that are attached to the apex of the delta wing [8]. These vortices can be seen in Figure 5-4 to attach to the upper surface of the wing along two lines inboard of the leading edges. The area between the two vortices is called the central core, and contains essentially two-dimensional flow of approximately free stream velocity. The area outboard of the vortex attachment lines is called the separation region. For the Reynolds numbers involved in this thesis, the separation region remains laminar and attached to the top of the wing [20]. This region has reversed flow that moves toward the leading edge.

Delta wings of low aspect ratio are analytically described as having conical flow. This means that the flow pattern in any plane transverse to the centerline of the wing has a similar form at all distances from the apex. Velocities along any radial line from the apex should be uniform for all distances. The assumption of conical flow has provided a number of recent developments in analytical delta wing research [8].

Figure 5-5 is a photograph of the wing vortices on a delta wing at 15° angle of attack, as seen from the front of the wing. The light sheet was placed perpendicular to the surface of a wing mounted on a sting. The camera was positioned perpendicular to the sheet. The outline of each vortex and the region of separation outboard of the attachment line can be noticed. The central core is marked by points of light as the particles move through the light sheet. The vortices are quite large, because the photograph was made near the trailing edge.

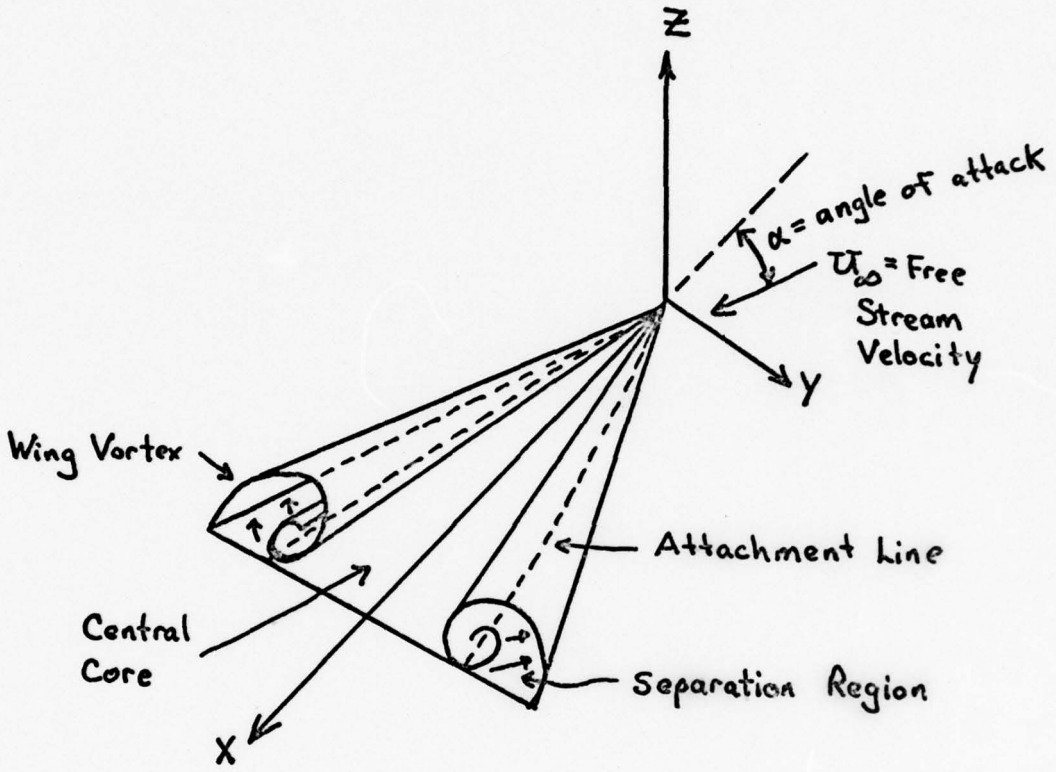

Figure 5-4

VORTEX SEPARATION ON A DELTA WING [8]

Figure 5-5

VORTICES NEAR TRAILING EDGE OF DELTA WING, $\alpha = 15°$

Figures 5-6 to 5-9 contain photographs made for $\alpha = 5°$, at various distances from the upper surface of the flat plate. The figures below each photograph show the velocity mapping in that two-dimensional plane.

Figure 5-6 was made at .2 mm depth. It can be noticed that the particles diverge laterally from the central core, where velocities are the order of 30 cm/sec. Velocities in this diverged area fall off to about 20 cm/sec. No attachment line is noticed since vortices are not formed at such a low angle of attack. Particles moving over the leading edge were deflected slightly from free stream direction. Deviations in streak length near the upper surface are caused by deposition of particles on the surface. In addition, the large velocity gradient near the surface in the z-direction produced deviations in streak lengths in a light sheet of finite thickness.

Photographs made every .2 mm indicated a gradual change in the flow pattern and velocities. Figure 5-7 was made at 2.0 mm from the upper surface. The flow has smoothed out considerably where the particles from the leading edge met the central core. Velocities in the central core rose to approximately 70 cm/sec and reduced to around 40 cm/sec near the outboard trailing edges. Lateral divergence from the central core remained at approximately the same level as near the surface.

Figure 5-8 was made at 5 mm depth. The flow was converging inward toward the central core, where velocities have risen to 80 cm/sec. The velocities remained uniform over a large area of the wing. Little effect can be noticed at the leading or trailing edges.

Figure 5-9 is a view perpendicular to the model edge, with the sheet bisecting the wing through the apex. The area shown is the central core, where the flow is essentially two-dimensional except for the first 20%

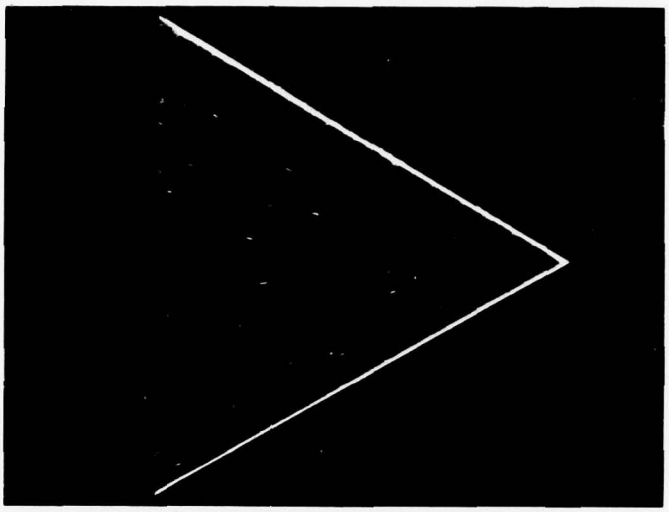

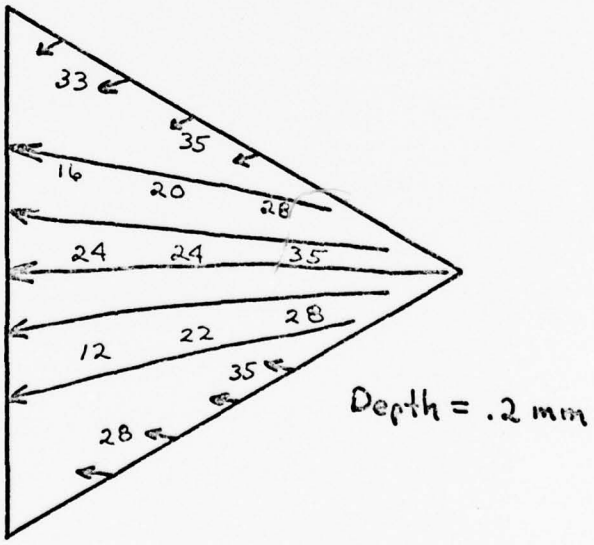

Figure 5-6

VELOCITY FIELD ON DELTA WING, α = 5°

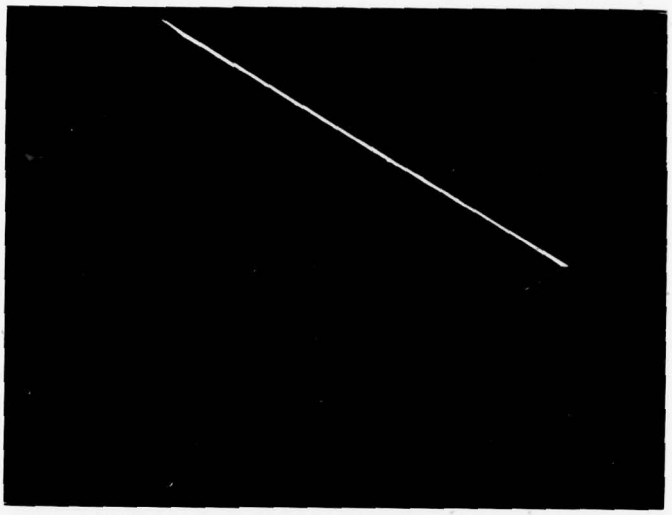

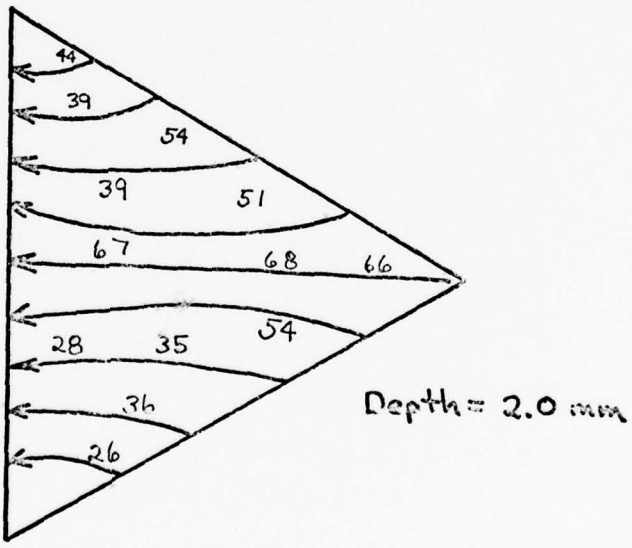

Figure 5-7

VELOCITY FIELD ON DELTA WING, $\alpha = 5°$

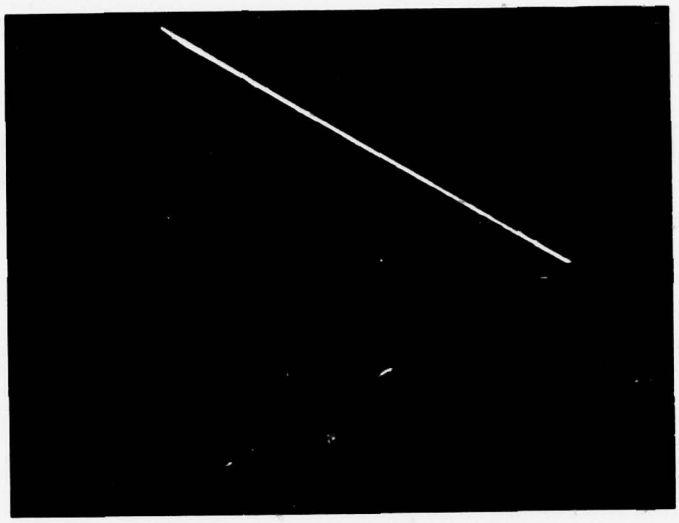

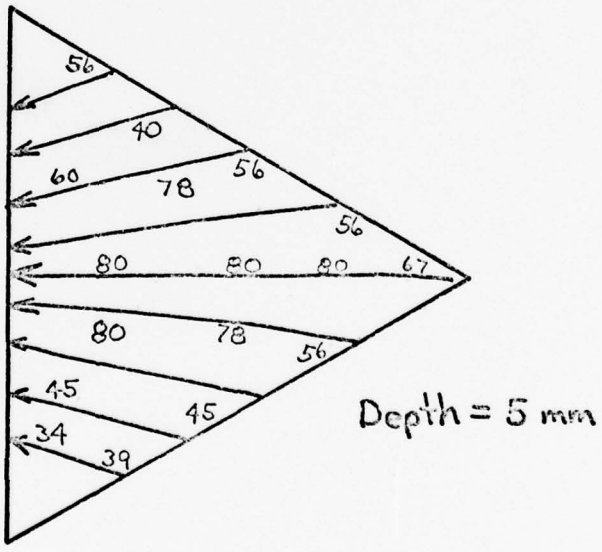

Figure 5-8

VELOCITY FIELD ON DELTA WING, $\alpha = 5°$

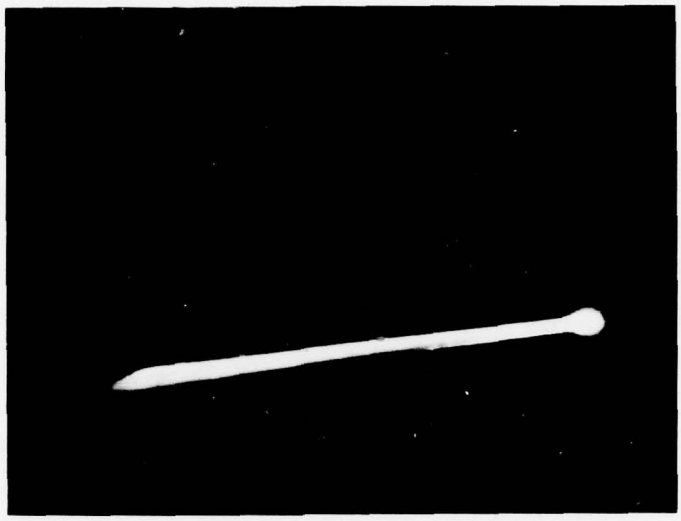

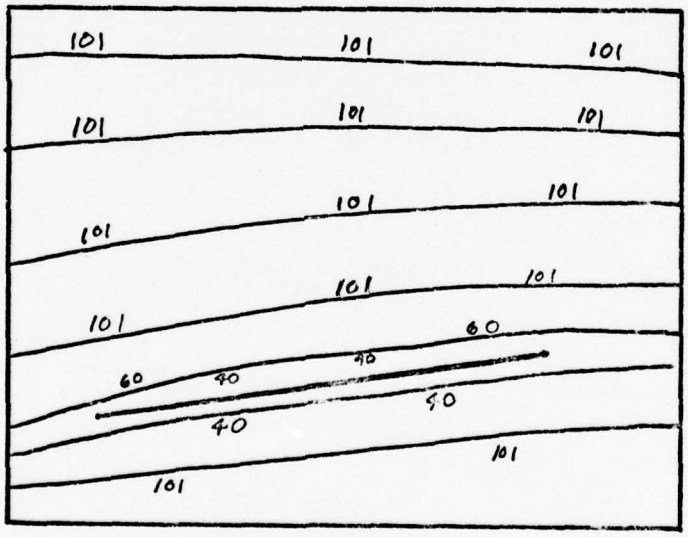

$\alpha = 5°$

Figure 5-9

VELOCITY FIELD ABOVE CENTER OF DELTA WING

chord point. The velocity gradient in the z-direction is apparent. Velocities from this view correlate with those found in the central core on the previous planform views.

The angle of attack was raised to 15° for the next set of photographs. Figure 5-10 was made at .2 mm depth. The attachment line of the two vortices and the separated region of reverse flow are clearly shown. The flow in the separation region hooked forward toward the leading edge at approximately 10 cm/sec. The central core had a high degree of divergence, but velocities remained over 60 cm/sec nearly to the attachment line.

Figure 5-11, at 2.6 mm depth, shows that the vortex attachment lines were less clearly defined over the first 30% of the chord. The light sheet was above the vortices for the first 30% of the chord, after which it penetrated the vortex, thus making the attachment lines. The separation region is faintly noticeable between the attachment line and particles inbound over the leading edge. Velocities in the separation region have risen to 17 cm/sec. Velocities in the central core have risen only slightly to 80 cm/sec.

At 5 mm depth, Figure 5-12 indicates that the light sheet was above the vortices up to the 50% chord point. No reverse flow is shown since the separation region was below 5 mm depth. Central core velocities rose slightly to 85 cm/sec and remained large over most of the wing. The vortices can be recognized as the two dark lobes downstream of the 70% chord point.

Figure 5-13 shows the two-dimensional flow above the central core. The separated region near the apex had increased to the 30% chord point. The effects of this separation can be seen in Figures 5-10, 5-11 and 5-12

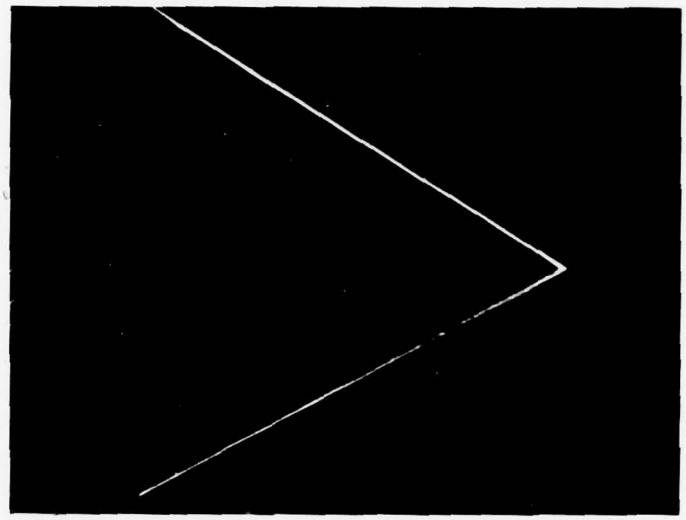

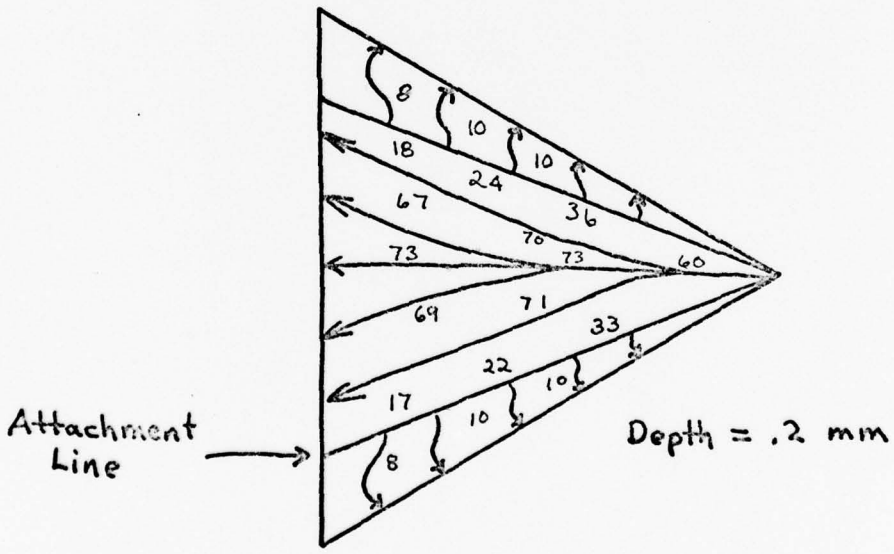

Figure 5-10

VELOCITY FIELD ON DELTA WING, α = 15°

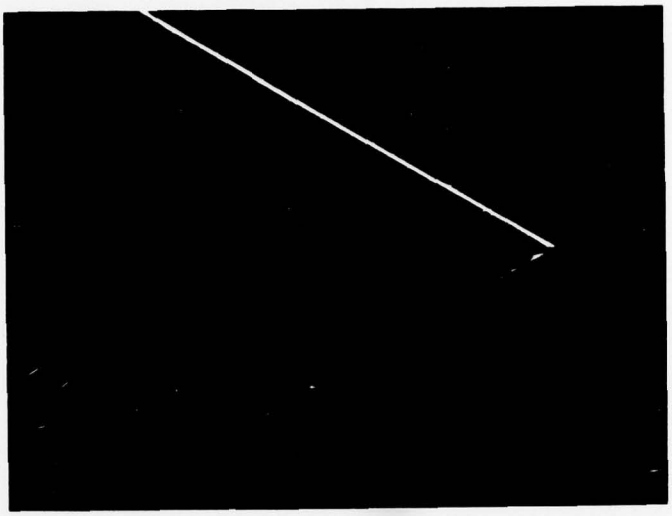

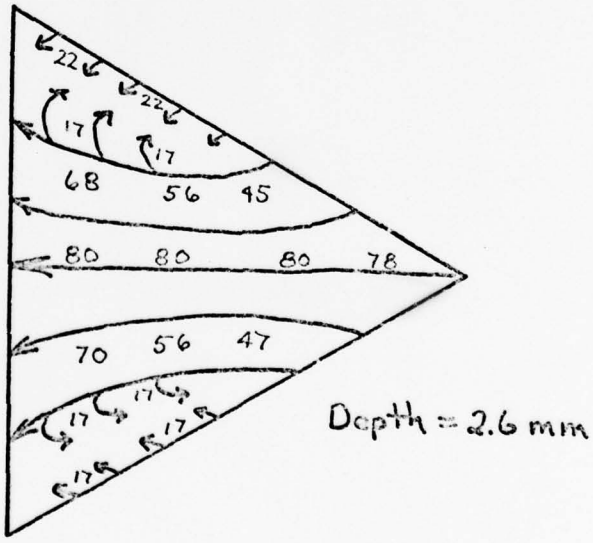

Figure 5-11

VELOCITY FIELD ON DELTA WING, α = 15°

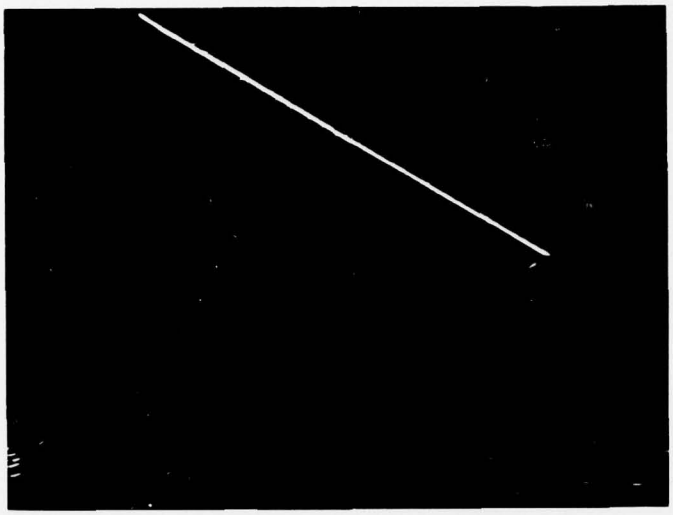

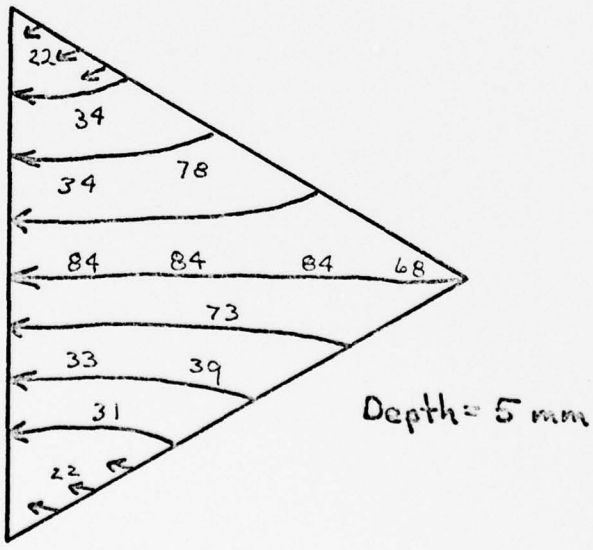

Figure 5-12

VELOCITY FIELD ON DELTA WING, α = 15°

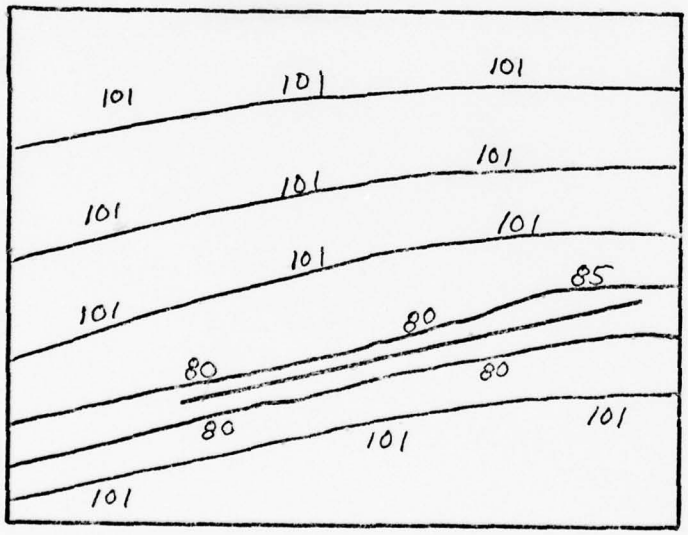

Figure 5-13

VELOCITY FIELD ABOVE CENTER OF DELTA WING, α = 15°

as a velocity less than that over the rest of the central core. This was caused by the arcing of the particles through the sheet, leaving a shorter streak.

The velocity gradient near the surface in the z-direction was greater at $\alpha = 15°$ than at $\alpha = 5°$. This is corroborated by the higher velocities at the .2 mm depth mapping for $\alpha = 15°$.

Photographs were made at $\alpha = 25°$, but the results were essentially the same as at $\alpha = 15°$, and thus will not be presented here.

5.4 Comparison of Results with Theory

An excellent analytical treatment for the flow over a delta wing of low aspect ratio is that by Smith [20]. His treatment was based on conical flow past a slender, flat delta wing without thickness, in which the wing vortices are represented by coiled vortex sheets in an irrotational flow. Smith's method uses an iterative scheme to solve the equations of motion on a computer. The only portion of the solution that can be compared here is the velocity on the upper surface. Smith based his treatment on a low aspect ratio wing of zero thickness with sharp edges. Although the 60° delta wing in this thesis has a medium aspect ratio, a finite thickness, and beveled edges, the results will nevertheless be compared to Smith's treatment.

Figure 5-14 is a plot of experimental data taken by LSV at $\alpha = 15°$. Also shown on the plot is Smith's analytical curve. The non-dimensional longitudinal velocity, u_*, is plotted versus position on the semispan. Since Smith assumed conical flow, the analytical results would be the same for any transverse plane on the chord. The flow is not conical on the experimental wing, thus several curves are shown for different positions

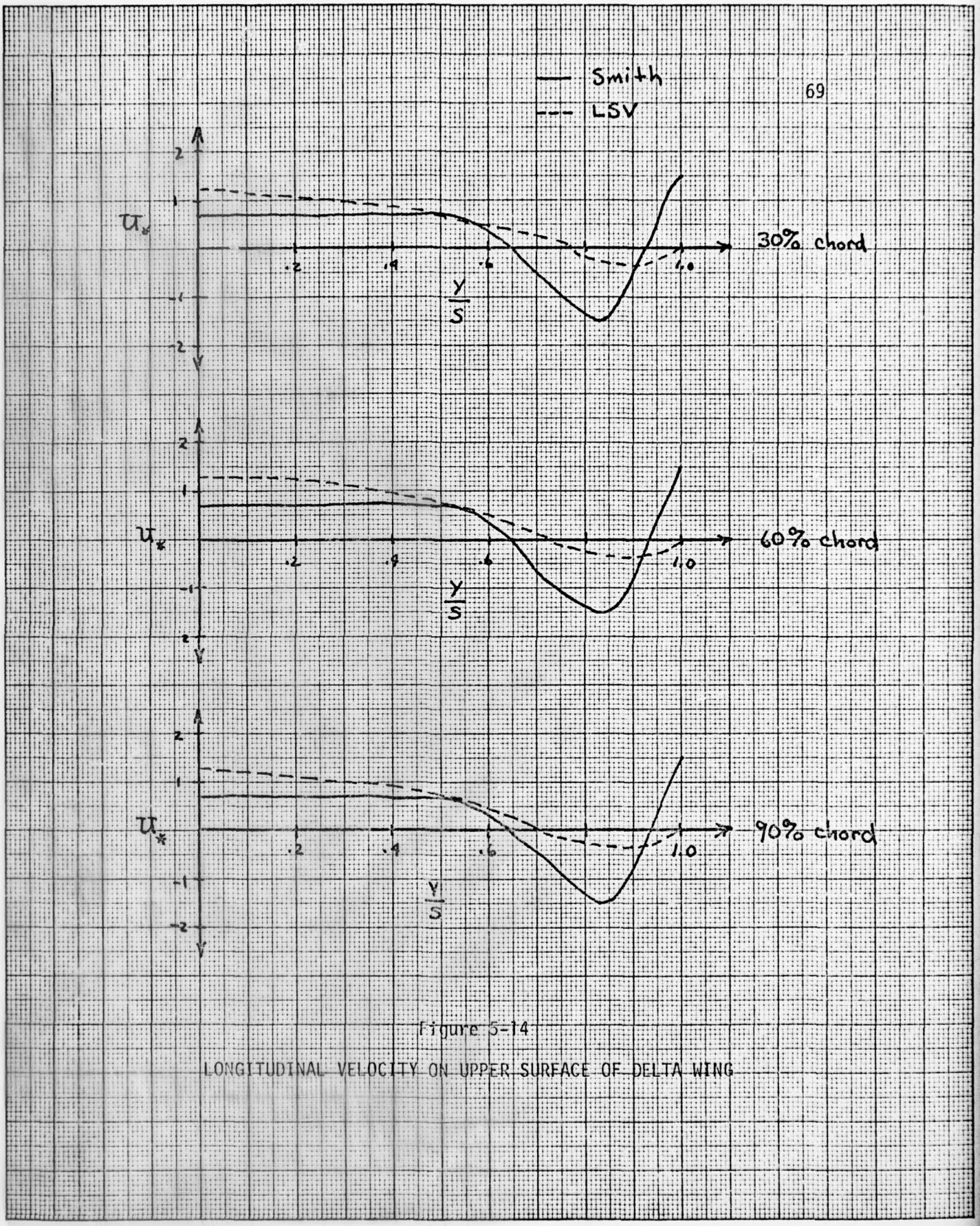

Figure 5-14

LONGITUDINAL VELOCITY ON UPPER SURFACE OF DELTA WING

on the chord. The experimental velocities were taken .2 mm above the surface of the wing. The non-dimensional longitudinal velocity, u_*, is

$$u_* = \frac{u}{kU_\infty} \tag{5.1}$$

where u = Longitudinal component of velocity on surface

K = tan γ

U_∞ = Free stream velocity.

The similarity parameter, a, as used on the plot is

$$a = \frac{\tan \alpha}{K} \tag{5.2}$$

where α = Angle of attack.

For $\alpha = 15°$, the experimental wing had a = .46. This is compared to the a = .50 theoretical plot of Smith.

It is shown that the actual flow on the delta wing is not strictly conical. The point of zero longitudinal velocity moves from 77% of the semispan at the 50% chord point to 70% of the semispan at the 90% chord point.

The reverse flow on the delta wing was not as great as predicted by theory, nor did the flow resume downstream movement before reaching the leading edge. These may be due to the fact that the 60 degree delta wing has a medium aspect ratio instead of a small aspect ratio as was Smith's assumption. The general shape of the plots are similar, the main differences being the magnitude of the reverse flow. A similar comparison for $\alpha = 5°$ cannot be made since no vortex separation occurred at such a low angle of attack.

Unfortunately, little theoretical information is available on velocities above the wing. Most analytical results are concerned with pressure distribution, vorticity or force moments, since these have classically been the easiest to measure for corroboration of theory.

5.5 Conclusion

The extremely complicated flow over a delta wing was measured by LSV. The velocity mappings provided a great amount of information on the flow in the two-dimensional flow above the wing. The attachment line, separation region, and vortex position could be delineated from the photographs.

The velocity on the upper surface was compared to a theoretical curve by Smith. The discrepancies between the two curves can be traced to the difference between the aspect ratios and his simplifying assumptions of conical flow and zero wing thickness.

The flow in the two-dimensional planes above the wing was not completely analyzed. There is a great deal of data in the photographs that can and should be analyzed, however, there is no corresponding theory for comparison.

The laser streak velocimetry technique could therefore be used to provide better empirical data on which to base improved analytical treatments.

Chapter 6

FUTURE DEVELOPMENTS

6.1 Introduction

This chapter will discuss some of the possible areas that could be pursued with this technique. These include improvements to the present method as well as extending laser streak velocimetry to three-dimensional measurements. The use of fluorescence and phosphorescence instead of elastic scattering will also be discussed.

6.2 Improvements to Present Method

The size and shape of the scattering particles has a great influence on the accuracy of the measurements. By reducing the size of the particles to approximately one micron, there would be substantial fidelity in following flows up to high subsonic speeds. The uniformity of the particle size should be increased to reduce variations in streak length due to lag.

The talc particles used in this thesis were irregular in shape. This caused variations in the intensity of single streaks due to the rotation of the particles at very low airspeeds. This was because the particle presented different geometric shapes to the light sheet as it rotated. This rotation was less apparent at airspeeds over 10 cm/sec. Spherical particles would prevent this problem from occurring.

The dispersal of particles into the flow should be automated. If liquid particles are used, several atomization processes such as the LaMer generator and sonic nozzles are available [5]. Solid particles would require a method of dispersal by vibration or entrainment in an air jet [7].

In any such method, care must be taken to avoid introducing turbulence or eddies into the flow.

More precise measurements could be made by making the light sheet thinner and more uniform in energy density. This would be most useful in mapping velocities with large gradients. The uniform illumination would prevent loss of information near the edges of the light sheet. Thinner sheets would require less laser power for the same energy density.

Streak lengths could be measured more accurately with a microphotodensitometer. The length could be designated as the distance between the half power points as digitalized by the microphotodensitometer.

6.3 Three-Dimensional Flow Measurements using LSV

When making many successive photographs at different distances from a body, the flow must be steady to get meaningful results. Thus, for unsteady or turbulent flows, the entire three-dimensional volume must be photographed in a very short time. The entire flow could be photographed quickly by scanning the sheet and photographing with a high speed movie camera, a possible setup shown in Figure 6-1. The second mirror and lenses could be mounted on a high speed translation device with a scan rate of 1 cm/msec. Individual frame exposure times could be reduced to the microsecond range using pulsed lasers, although it would take a very fast flow to make such a short exposure time useful.

The individual photographs from such a high speed scan could be analyzed to provide a nearly instantaneous three-dimensional velocity mapping of a flow.

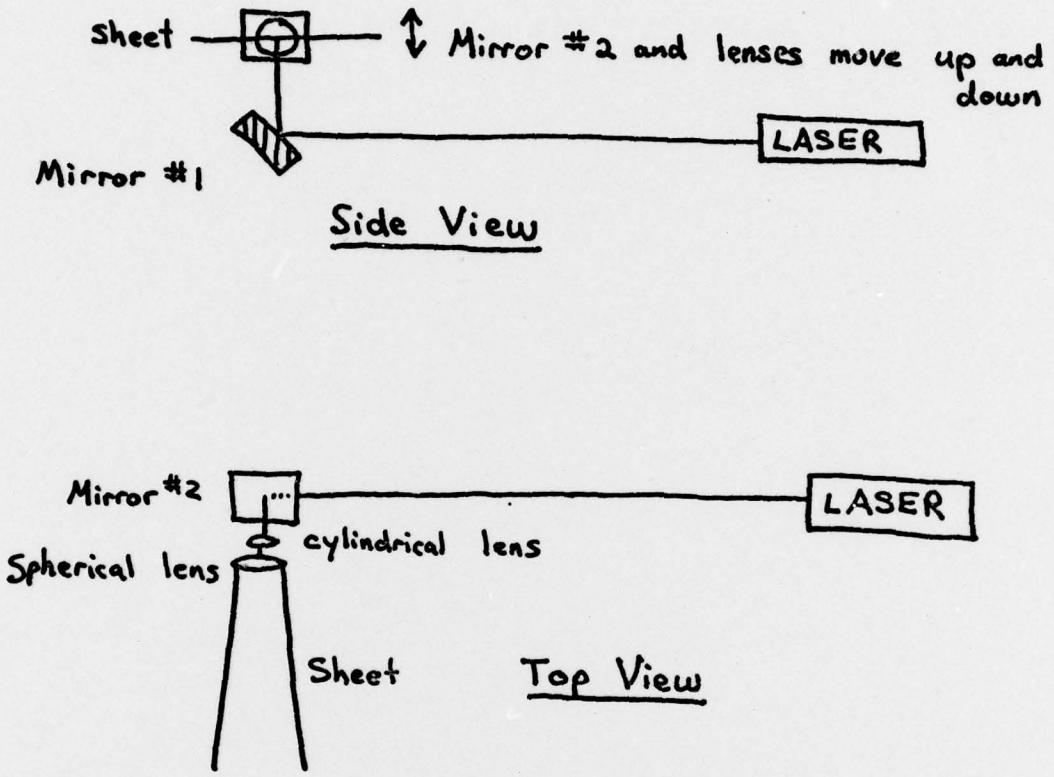

Figure 6-1

HIGH SPEED SCAN SETUP FOR LSV

6.4 Use of Fluorescent or Phosphorescent Particles

The use of fluorescent particles could be used in arrangements where reflections from the body cannot be eliminated by polaroids. Such a point is shown in Figure 5-13, where the glare from the wing apex masks the flow near the surface. By using fluorescent particles, the light from the laser could be filtered out and the fluorescent light from the particles passed to the camera. This is possible because the fluorescent particles absorb light from one wavelength region and emit fluorescence in another region. The time lag for absorption and emission is typically 10^{-8} seconds [9]. This makes fluorescence useful for high speed flows.

In earlier experiments, Rhodamine 6G, a laser dye, was dissolved in water and a small droplet placed on the flat plate model. It was excited with laser light of 5145 angstroms. The fluorescence was clearly visible to the naked eye when viewed through a sharp cutoff filter. However, the fluorescence intensity emitted near 5600 angstroms by the dye was too weak to register on the camera film at F/4.5 and 1/15 second. Other dyes of larger quantum efficiency may be useful in this respect.

An alternate method would use phosphorescent particles, whose lifetime is on the order of milliseconds. The absorption and emission process is somewhat similar to fluorescence, except for longer lifetimes. In this case, the decay time of the particle could be used as the mechanism to produce streaks. [21]. For a given lifetime, faster flows would produce longer streaks.

This method would not require a sheet, but only a single Gaussian beam focused to a small waist with a very high energy density. Particles passing through the waist would absorb enough energy to leave visible streaks

downstream.

The waist could be moved across a two-dimensional plane in a raster scan that would map the velocities in that plane. If the waist were translated as well as scanned, the velocities in a volume would be mapped. Such a scan would require orthogonal cameras or electronic image sensing devices since there is no longer a sheet to define one plane. The electronic image sensing devices could be connected to a computer for instantaneous printout of the three-dimensional velocities.

Unfortunately, most substances that phosphoresce, do so at temperatures near 77°K [9]. Butandione, a yellow liquid food coloring additive, is an exception. In this research, it was atomized in a jet stream and excited by 4579 angstrom laser light. A definite streaking was noticed downstream of the laser beam. The noxious and long lasting odor made it impractical for use in an open loop tunnel system as was used in this research.

6.5 Conclusion

The LSV method could be improved by making the particles uniform one micron spheres, designing an automatic particle dispersal system, and by reducing the thickness of the sheet. High speed scnnning of the sheet would extend the method to mapping nonsteady, three-dimensional flows. The use of fluorescent and phosphorescent particles may provide an alternative to elastic scattering particles. Each of these areas should be investigated for validity.

Chapter 7

CONCLUSION

Laser streak velocimetry has been introduced as a method of quantitatively and qualitatively analyzing the flow around aerodynamic shapes. The velocity and visualization measurements were in good agreement with theory and other experimental data.

LSV was used to measure the velocity profile in a boundary layer on a flat plate. The results were within an average of 4% of the theoretical value when the longest streaks over a region were used.

The wake behind a circular cylinder was analyzed for Reynolds numbers of 70-300. The wake length measurements at low Reynolds numbers were found to agree closely with theory up to Re = 70. At Reynolds numbers greater than 70, LSV measurements agreed with other experimental data.

The velocities in the wake of a cylinder at Re= 90 were mapped. The velocities in a transverse plane were compared to previous experimental work done with a hot wire anemometer. LSV measurements were closer to the theoretical values expected.

Separation angle on a circular cylinder was measured at Re = 300. Results were very close to the theoretical value of 82° from the forward stagnation point.

Instantaneous velocities in the shedding vortices behind a circular cylinder was mapped at Re = 270. Individual vortices and their velocity gradients were graphically evident.

The flow over a 60° delta wing at 5°, 15° and 25° angle of attack was presented. The surface velocities were compared to previous analytical

predictions and found to agree substantially. The velocities above the surface in the central core were plotted up to 5 mm from the surface.

The LSV method dramatically showed the attachment line of the wing vortices, the reversed flow of the separation region, and the general shape and position of the vortices. Two-dimensional velocity mappings were constructed at .2, 2 and 5 mm from the surface. There was a great amount of data on the photographs that was not analyzed.

Laser streak velocimetry has definite advantages over previous velocity measuring methods. The requirement for only a laser and camera is a definite asset. Since most wind tunnels already have viewing windows, the technique could be applied to existing facilities with few modifications. There is minimal flow disturbance with LSV because no probes are inserted into the flow.

This technique produces graphic results that can be used to measure the velocities, visualize the flow, and provide a permanent record at the same time. It should be especially useful for instruction in aeronautics and fluid mechanics.

There are certain limitations to LSV. It works best with essentially two-dimensional flows, but could be used to make a three-dimensional mapping with a high scan rate. The method is restricted to incompressible flows, since there would be appreciable particle lag when passing through shocks [3]. The size and shape of the particles will have a definite impact on the accuracy of results. Data reduction also becomes a problem when measuring complicated flows.

Overall, laser streak velocimetry has more advantages than limitations, and the potential for major breakthroughs in high speed velocity

mapping. It should prove to be a valuable tool for the aeronautical engineer.

REFERENCES

1. Jackson, D. A. and Paul, D. M., "Measurement of Hypersonic Velocities and Turbulence by Direct Spectral Analysis of Doppler Shifted Laser Light," Physics Letters, Vol. 32A, Number 2, 15 June 1970.

2. Goldstein, R.J., "Measurement of Fluid Velocities by Laser-Doppler Techniques," Applied Mechanics Reviews, Vol. 27, No. 6, June 1974.

3. Mazumder, M. K. and Kirsch, K. J., "Flow Tracing Fidelity of Scattering Aerosol in Laser Doppler Velocimetry," Applied Optics, Vol. 14, No. 4, April 1975.

4. Hulst, H. C. Van de, Light Scattering by Small Particles, John Wiley and Sons, Inc., New York, 1957.

5. Green, H. L. and Lane, W. R., Particulate Clouds: Dusts, Smokes, and Mists, 2nd Edition, E. & F. N. Spon Ltd., London, 1964.

6. Hidy, G. M. and Brock, J. R., The Dynamics of Aerocollodial Systems, Pergamon Press, New York, 1970.

7. Fuchs, N. A., The Mechanics of Aerosols, Revised and Enlarged Edition, MacMillan Co., New York, 1964.

8. Batchelor, G. K., An Introduction to Fluid Dynamics, Cambridge University Press, London, 1967.

9. Pringsheim, P., Fluorescence and Phosphorescence, Interscience Publishers, Inc., New York, 1949.

10. Schlichting, H., Boundary-Layer Theory, 6th Edition, McGraw-Hill Book Co., New York, 1968.

11. Nishioka, M. and Sato, H., "Measurements of velocity distributions in the wake of a circular cylinder at low Reynolds numbers," Journal of Fluid Mechanics, Vol. 65, Part 1, 1974.

12. Lamb, H., Hydrodynamics, Dover Publications, New York, 1932.

13. Yih, C., Fluid Mechanics, McGraw-Hill Book Co., New York, 1969.

14. Dennis, S. C. R. and Chang, G., "Numerical solutions for steady flow past a circular cylinder at Reynolds numbers up to 100," Journal of Fluid Mechanics, Vol. 42, Part 3, 1970.

15. Jones, W. P., "Trends in Unsteady Aerodynamics," Journal of the Royal Aeronautical Society, Vol. 67, No. 627, March 1963.

16. Orloff, K. L. and Grant, G. R., "The Application of Laser Doppler Velocimetry to Trailing Vortex Definition and Alleviation," NASA Technical Memorandum, Number NASA TMX-62, 243, February 1973.

17. Fink, P. T. and Taylor, J., "Some Early Experiments on Vortex Separation," British Ministry of Aviation, Aeronautical Research Council Reports and Memoranda, R. & M. No. 3489, 1955.

18. Peckham, D. H., "Low Speed Wind Tunnel Tests on a Series of Uncambered Slender, Pointed Wings with Sharp Edges," British Ministry of Aviation, Aeronautical Research Council Reports and Memoranda, R. & M. No. 3186, 1954.

19. Mangler, K. W. and Smith, J. H. B., "Calculation of the Flow past Slender Delta Wings with Leading Edge Separation," Royal Aircraft Establishment, Report No. Aero. 2593, May 1957.

20. Smith, J. H. B., "Improved Calculations of Leading-Edge Separation from Slender Delta Wings," Royal Aircraft Establishment, Technical Report No. 66070, March 1966.

21. Epstein, A. H., "Quantitative Density Visualization in a Transonic Compressor Rotor," Ph.D. Thesis, Department of Aeronautics and Astronautics, Massachusetts Institute of Technology, September, 1975.